Homogenization techniques in Digital Rock Physics

Revisiting the Hill-Mandel principle and determination of the evolution law of the convergence cone

Sijmen Zwarts

Delft University of Technology

TU Delft

Homogenization techniques in Digital Rock Physics

Revisiting the Hill-Mandel principle and determination of the evolution law of the convergence cone

by

Sijmen Zwarts

to obtain the degree of Master of Science
at the Delft University of Technology,

Student number:	4969480	
Project duration:	April, 2022 – May, 2023	
Thesis committee:	Dr. M. Lesueur,	TU Delft, supervisor
	Prof. Dr. Ir. L. J. Sluys,	TU Delft
	Dr. O. Colomés,	TU Delft
	Dr. H. Hajibeygi,	TU Delft

An electronic version of this thesis is available at `http://repository.tudelft.nl/`.

TU Delft

Acknowledgements

It is with great pleasure and gratitude that I present this thesis, which marks the culmination of years of hard work, research, and personal growth. I would like to express my sincere thanks to the many individuals who have helped me along the way.

First and foremost, I would like to thank my parents, whose unwavering support have been the foundation of my academic journey. They have always encouraged me to pursue my passions and dreams. Without their guidance and encouragement, I would not be where I am today.

I would also like to extend my gratitude to my supervisors, Martin in particular, for their guidance, mentorship, and expertise. Their encouragement and insightful feedback have pushed me to become a better researcher and writer. Their commitment to my success has been unwavering, and I am grateful for their support.

Furthermore, I would like to acknowledge the many individuals who have provided me with invaluable assistance and encouragement throughout my research, in particular Kari, Titia and Ruben. Their contributions have been instrumental in helping me to refine my ideas, overcome obstacles and achieve my goals.

Overall, I am deeply grateful to all of the individuals who have supported me on this journey. This thesis would not have been possible without their support and encouragement and I hope that my work will serve as a testament to their faith in me.

Sijmen Zwarts
Delft, May 2023

Summary

The first part of the thesis explores the process of homogenization, particularly for the permeability properties of rock samples. The Hill-Mandel postulate of energy consistency throughout the transitioning of scales is revisited since traditional homogenization methods rely on applying specific boundary conditions to enforce energy consistency. However, it is shown that the applied boundary conditions influence the effective physical parameter and provide upper or lower bound estimations. Recently, it is shown that these boundary conditions influence a layer near the boundary of the sample and that homogenization applied on the subsample away from this boundary layer is not affected by the boundary conditions.

The research focuses on energy consistency by studying the evolution of the energy within the intrinsic subsample, away from the boundaries. With the help of Finite Element simulations of Stokes-flow through idealized structures, the energy of the fluid is traced without the influences of grain properties on the energy dissipation. By plotting the ratio of the energy dissipation of the macro- and micro-scale, it is shown that the energy consistency is not found within small subsamples. Yet, with a growing subsample, energy consistency is achieved naturally, without the enforcement of boundary conditions. As a result, it is concluded that the energy consistency is found at the Representative Elementary Volume (REV), which is a similar requirement as for traditional homogenization methods. The study of the natural energy consistency in idealized microstructures is extended to real microstructures, which include more natural heterogeneities, such as grain properties. It is shown that energy consistency is also found with the natural heterogeneities included, albeit with a slower convergence.

For the homogenization of the permeability of a sample, the energy ratio is now known to be unitary, which can be used as an accurate indicator to determine the size of the REV.

The second part of the thesis explores the process of determining the size of the REV, which is a common, yet essential practice in Digital Rock Physics. Currently, this is an extensive exercise, involving many and large-size simulations to trace the convergence of the physical property and requires a lot of computational resources and time. Numerical-statistical studies have shown that the convergence of the REV visualizes in a cone-like shape. By plotting the convergence for both the permeability and the energy dissipation ratio for idealized microstructures, this study analyses the shape and evolution of the cone of convergence. From this, the generic evolution law of the convergence is determined.

It is shown that the asymmetrical convergence cone is described with a log-normal distribution, with a stable mean throughout the evolution of the cone and a variance for each sample size. The evolution of the variance is described with the law of large numbers, taking into account a reference value. This makes it possible to determine the size of the REV. Since the statistical method applies, information about the error of the fit, the error of the determined homogenized property, and the error of the size of the REV is provided.

The study is extended to real microstructures to validate whether the determined evolution law applies when natural heterogeneities are included. It is shown that the evolution law still accurately describes the REV's convergence. Therefore, the REV's size of real rock samples can also be determined. Even when the REV is not included within the sample, the evolution law can provide an estimate of the size of the REV or the homogenized property.

By using the cone of convergence, it is not necessary to run simulations on the full sample to find the REV, which is computationally expensive, instead running a number of simulations on small subsamples is sufficient, which saves both time and computational resources. It also unlocks the possibility to find the REV for high-resolution samples, as splitting the sample into subsamples allows for smaller simulations.

Contents

1 Introduction

1.1. Research context

Digital rock physics is a field of study that involves the digital analysis of rock samples. As the computational power and modelling capabilities improved, researchers have developed digital models to study rock behaviour under different conditions, such as the flow of fluids through rocks or the deformation under stress.

Digital rock physics usually follows a couple of steps to study the behaviour of the rock. It starts with image acquisition. A three-dimensional rock image is created with the use of X-ray computed tomography on a real rock sample. The next step is to translate the images into phases, such as the pores and grains. Once the phases are segmented, the rock can be reconstructed into a three-dimensional computational model, which usually involves creating a mesh of the voxels or pixels. In the next step the behaviour of the rock to any type of physical process, such as fluid flow, stress or heat transfer, can be analysed with simulations on the computational models. With the results of the simulation, homogenization of the properties can be applied to larger scales. The properties need to be translated to larger scales, since the complex microstructure of the rock, containing the segmented voids and grains, is heterogeneous and modelling large-scale structures with the microstructure is impractical, as the complexity of the microstructure requires high computational power. In order to model larger structures for larger applications, a homogeneous equivalent of the material is created through homogenization of the microstructure.

Homogenization is a mathematical process which analyses the properties and the physical response of the microstructure to a physical process and computes the effective properties on the macroscale. To connect the two different scales, homogenization falls back on the thermodynamic law of energy consistency throughout the scale transition, also known as the Hill-Mandel principle. The average energy of a volume on the microstructure is processed and matched with the energy of a volume on the macroscale. The volume in which this energy consistency is found is called the Representative Elementary Volume (REV).

To apply valid homogenization, the characterisation of the REV is a critical step in digital rock physics, as this is the volume of the medium which on average accurately represents the behaviour of the rock on the macroscale. The effective property oscillates considerably when small volumes are homogenized but stabilizes with growing subsamples which on average contain enough complexity of the microstructure to represent the medium. Thus, by running simulations on growing subsamples and postprocessing the properties, the oscillation of the effective properties will dampen out and the size of the REV can be determined. In some cases, such as with material softening and crack evolution, the existence of the REV is questioned (Gitman, Askes, and Sluys [15]; Lacy, McDowell, and Talreja [22]). Although, it is shown that the REV for linear problems and material hardening can be determined.

Another benefit of the REV is the applicability of multiscale modelling. The homogenized property

is used to model the macroscopic scale, which in its turn provides input for the boundary value problem of the microscale. This circular system enables the possibility to model complex problems, such as non-linear physical responses in the material behaviour without making any assumptions in the constitutive law.

1.2. Problem definition

In homogenization schemes, the energy is divided into an average field and a fluctuation field. Since the REV is the volume that contains stabilized energy ratio throughout the transition of scales, the fluctuation field has to become zero and the average energy field is used to compute the effective properties. Currently, the homogenization schemes enforce the fluctuation of the energy to be zero with specific boundary conditions. However, it turns out that these boundary conditions influence the effective property of the medium (Andrae et al. [2]; Guibert et al. [18]; Gerke, Karsanina, and Katsman [12]; Shi et al. [47]; Zakirov and Khramchenkov [51]). The kinematic or dynamic boundary conditions provide an upper and lower bound estimation of the property. Thovert and Mourzenko [48] showed that homogenization applied on a subvolume, away from the boundaries, will not be affected by the boundary conditions, as the computed permeability of the samples converges towards the same value. Therefore, it is natural to question if energy consistency throughout the transition of scales can be found within the subsample away from the boundary layer. This would make the boundary conditions to enforce the energy consistency otiose and could provide a REV for which the homogenized properties are stabilized and not influenced by upper or lower bound estimations.

Another problem in the process of finding effective properties lies within the process of finding the size of the REV. As described, the process of finding the REV involves running multiple simulations on growing subsamples, sometimes including large or high-resolution samples. This is a computationally expensive process, as many simulations can take a long time to complete and simulations on large samples require a lot of computational resources and time on itself. Furthermore, it is unknown to which value the effective property converges, which makes it complicated to know when the REV has been found. Many studies have been done to optimize the process and define the REV through different methods. Some researchers have shown that the REV for a specific material and its physical properties can be related to the size of the material or the number of grains in the volume. These indicators for the size of the REV, however, change when other materials or properties are considered. Other researchers took a numerical-statistical approach, which shows the convergence through the variance of the property. It is shown in these studies that plotting the REV convergence results in a cone of convergence, starting with a large base considering small samples and converging towards a certain value when larger volumes are considered. The evolution law of the convergence would make it possible to predict the size of the REV without the need for large-scale simulations and unlock the possibility to work with high-resolution samples. On top of that, the description of the cone provides an estimation of how accurate the determination of the size of the REV and the homogenized property is, due to the decreasing width of the cone.

1.3. Goals and objectives

1.3.1. Goals

The first goal of this research is to perform a study with an intrinsic subvolume and analyse the behaviour of the energy within the subvolume away from the boundary. By plotting the energy ratio from micro- to macro-scale, it is possible to determine if the energy consistency can be found naturally. The result provides a method to apply homogenization without enforcing energy consistency and therefore apply upscaling in a natural way, without upper- or lower-bound estimations.

The second goal of this research is to plot and analyze the REV convergence. From this, the evolution law of the convergence for the REV can be determined and described mathematically. The determined evolution law can be applied and verified on increasingly heterogeneous samples. The result of this study provides a new method to determine the size of the REV and the homogenized property quickly and efficiently.

1.3.2. Research questions

This leads to the following research questions:

1. Can homogenization be done inside a subsample, with energy consistency though-out the transition of scales, without the influence of the boundary conditions?
2. Is it possible to determine the generic evolution law of the REV convergence and extrapolate it to real microstructures to predict the REV of a real structure?

1.3.3. Objectives

To achieve the goals of this thesis, the following objectives are set:

1. Set up a model to determine both the permeability and the energy dissipation of the fluids in a subsample away from the boundary, using idealized microstructures to remove influences of the grain properties.
2. Determine the evolution of both the permeability and the energy dissipation of the fluids and analyse the evolution to confirm if natural energy consistency can be found within the subsample and analyse the convergence towards REV.
3. Define a method to apply homogenization with the natural energy consistency ratio and define the evolution law of the convergence to REV.
4. Apply the methods on real microstructures and analyse the influence of the grain heterogeneous properties on the methods.

1.4. Research outline

The outline of this thesis differs from a standard Master Thesis, as both research questions are answered in paper form. Therefore, this thesis is a merge of the two articles, together with an introduction to the thesis, a conclusion, and a summary.

The outline of the thesis looks as follows:

- The second chapter is the article ‘Finding the Representative Elementary Volume using the conservation of energy across scales’.

  In this article, the first research question is answered. The Stokes-flow model and the method to trace the convergence of the energy dissipation and permeability are described in this paper.

- The third chapter is the article ‘Predicting the Representative Elementary Volume by determining the evolution law of the cone of convergence’ article.

  This article answers the second research question. The convergence for REV is plotted and analysed. An evolution law for convergence is determined and applied to both idealized microstructures and real rock samples.

- In chapter 4 the conclusions of both articles are combined and listed.
- In Appendix A a more in-depth explanation of the model setup is provided.

1.5. Research scope

To successfully answer the research questions in the time provided for the Master Thesis, the following scope is defined for this research:

Since the first part of this study focuses on energy consistency throughout the transitions of scales, it is necessary to define which energy. Permeability is arguably one of the most important properties of Digital Rock Physics, therefore this study will limit itself to the energy dissipation of the fluids. For the convergence of the REV, the same data is taken into account, and therefore the analysis of the evolution of the REV is limited to the permeability and energy dissipation ratio.

The results of this research may apply to multiple fields of interest, yet the starting point of the research is Digital Rock Physics, and therefore only idealized or real rock structures will be taken into account.

This research does look at the energy consistency within a subvolume. The size of this subvolume is determined for each model, but a relationship with the morphological parameters or the boundary conditions is outside the scope of this research.

2

Finding the REV using the conservation of energy across scales

Abstract

The foundation of homogenisation methods rests on the postulate of Hill-Mandel, describing energy consistency throughout the transition of scales. The consideration of this principle is therefore crucial in the discipline of Digital Rock Physics which focuses on the upscaling of rock properties.

For this reason, numerous studies have developed numerical schemes for porous media to enforce the Hill-Mandel condition to be respected. The most common method is to impose specific boundary conditions, such as periodic ones. However, the recent study of [48] has shown that most boundary conditions still result in the same intrinsic effective physical property if the averaging is applied outside the range of the boundary layer.

From this discovery, it becomes logical to question the status of Hill-Mandel postulate in porous media when homogenising away from the boundary.

In this contribution, we simulated Stokes flow through random packings of spheres and a range of rock microstructures. For each, we plotted the evolution of the ratio micro- vs macro-scale of the energy of the fluid transport outside the boundary layer, for a growing subsample size of porous media. Here, we prove that we naturally find energy consistency across scales when reaching the size of the Representative Elementary Volume (REV), which is a known condition for rigorous upscaling.

Furthermore, we show that this ratio for the energy consistency is a more accurate indicator of REV convergence since the mean value is already known to be unitary.

Keywords

Homogenization, Energy Conservation, Representative Elementary Volume

2.1. Introduction

In an attempt to reduce and replace destructive experiments, the goal of Digital Rock Physics (DRP) is to determine the physical response of the rock at the macro-scale, using simulations on the digitized microstructure. Indeed, it is widely acknowledged that physical rock properties are mainly determined by the geometry and arrangement of grains at the microscale, under the concept of structure-property relationships. For example, rock permeability, which is the focus of this contribution, has been shown to be influenced by the grain shape (D. C. Beard [9]). The characterization of permeability has later been extended to more morphological parameters of the rock microstructure (Cox and Budhu [8]; Torskaya et al. [49]). Given the existence of scale separation between the microscopic level, obtained with CT-imaging, and the macro-scale, rock properties can be obtained with homogenisation methods (Auriault

[3]).

The foundation of homogenization methods rests on the Hill-Mandel (Hill [19]; Mandel [27]) principle, which states that energy cannot be created or destroyed in a closed system and thus remains consistent. In the context of homogenization schemes, the principle is applied by conserving energy throughout the transition of scales, which means that the energy of the different scales should be identical to be able to apply homogenization from the lower scale. As the local energy inside the heterogeneous microstructure can spatially vary significantly, usual homogenization procedures apply the variation principle and split the energy into an average and fluctuation term. Only when the fluctuation of the energy becomes zero does the homogenized energy of the micro-scale have energy consistency across the scales and can be considered representative of the larger scale. Therefore, this volume can be used to create a homogeneous equivalent medium for the larger scale and makes it possible to determine effective properties of the rock sample, such as permeability. To make sure that the fluctuation of the energy is zero, current homogenization schemes impose specific types of boundary conditions.

For the homogenisation of permeability, which is a hydraulic property, we are looking at the work energy of the fluid transport. It is shown that this energy consistency is enforced by applying kinematic, traction or periodic boundary conditions (Boe [5]; Renard and Marsily [43]; Du and Ostoja-Starzewski [10]; Paéz-García, Valdés-Parada, and Lasseux [33]). However, those different boundary conditions significantly influence the effective homogenized permeability of the rock sample. By imposing either a pressure gradient or a constant flux boundary condition, the flow path becomes linear, which has a direct effect on the permeability tensor (Pouya and Fouche [40]). The more the medium enables the water in the direction of the pressure gradient, the more the permeability in that direction will be, and vice versa. Similar effects are shown by applying closed walls, periodic flows or slip boundary conditions, as the permeability is influenced in both direction and magnitude (Andrae et al. [2]; Guibert et al. [18]; Gerke, Karsanina, and Katsman [12]; Shi et al. [47]; Zakirov and Khramchenkov [51]).

To overcome this limitation in homogenization, we refer back to the foundational paper of Hill [19], who states that 'the fluctuation of the mean becomes insignificant within a few wavelengths of the surface and the contribution of the surface layer becomes negligible by taking the sample large enough'. This means that upon increasing the sample size, the homogenized property will converge to the effective property, despite the different boundary conditions. Note that the size where convergence is reached is called the Representative Elementary Volume (REV). This concept has recently been shown by Thovert and Mourzenko [48], which studied the influence of the boundary conditions when determining the transport coefficients of a sample. The study shows that the effective permeability of an intrinsic sub-volume, away from the boundary, appears to be identical, despite considering different boundary conditions. However, when the boundary layer is taken into account, the permeability will vary due to the different boundary conditions implemented. For example, the mean permeability can be up to ten times higher than the effective property when Dirichlet boundary conditions are applied on all the boundaries. On the other hand, it is observed that when the boundary conditions are applied on an extension of the sample, the homogenized permeability is influenced within a boundary layer eight times smaller than the Dirichlet boundary conditions and the homogenized permeability is only influenced by half the value of the effective permeability.

It is recommended to compute the effective permeability inside an intrinsic volume, away from the boundary layer, such that the boundary conditions have no influence on the homogenized parameter. Therefore, it becomes logical to question the purpose of the boundary conditions currently deemed necessary for homogenization schemes to enforce energy consistency throughout scales. Indeed, we expect the energy dissipation of the fluids to be influenced in a similar way to the fluid flow by the boundary conditions. Therefore, we wonder what becomes of the energy consistency across the scales in the intrinsic volume, away from the boundary. Is the Hill-Mandel principle still respected away from the boundary layer, unaffected by the boundary conditions?

This article is set up as follows. The second chapter presents how the models are set up and which methods are used to trace the energy dissipation. The third chapter is dedicated to applying the theory to real microstructures to verify if the results found are affected by natural heterogeneities.

2.2. Theoretical study

Since we mentioned in the previous section that the grain shape, grain roughness and other morphological parameter have a strong influence on the permeability, we also expect them to have a direct influence on energy dissipation. Therefore, the random packing of spheres is selected as the porous medium for this study. It represents a granular rock microstructure, with spheres instead of grains. The advantage we target by using this medium is that the equivalent grains have an idealised shape and therefore do not have any heterogeneities, preventing as intended any fluctuation of the permeability (Bijeljic et al. [4]). This would be peripheral to the core objective of this study. Furthermore, the porosity of the microstructure is controlled by the packing fraction, allowing to create different models.

2.2.1. Modelling porous media

The distribution of the spheres in the packing is generated with the OpenMC Monte Carlo code (Romano et al. [44]). To reduce the computational resources, we take a single 2D cross-section from each generated sphere packing as our idealized microstructure. It has been shown that the simulated fluid behaviour is similar in 2D and 3D, with the exception of the velocity magnitude, which is higher in the 3D simulations (Marafini et al. [28]). Since this study focuses on the conservation of energy across the scales rather than the exact permeability value, a 2D cross-section of the 3D sphere packing is sufficient. Gmsh (Geuzaine and Remacle [13]) is used to create the mesh for the cross-section, with triangular elements and a specified mesh element size.

The simulations on the microstructures are conducted with Navier-Stokes equations. The Navier-Stokes equations incorporate both the momentum and mass balance of the fluid. Assuming incompressible fluids, the lack of body forces and stationary solutions, which is the most common environment for fluid transport in the subsurface, one will automatically arrive at Stokes flow:

$$\mu \nabla^2 v - \nabla p = 0$$
$$\nabla \cdot v = 0$$

MOOSE (Permann et al. [35]; Peterson, Lindsay, and Kong [36]) is used to implement the Stokes-flow simulations, following the framework of Lesueur et al. [24]. The flow is imposed through a predetermined pressure gradient across the domain. The classical no-slip condition is applied to the grains inside the sample. The external boundary conditions do not matter, since the focus of this study is on the postprocessing of properties away from the boundary layer, unaffected by the boundary conditions. Thus, a standard no-slip condition is applied to the external boundaries. An example of the flow through a cross-section of a random packing is shown in Figure 2.1.

2.2.2. Permeability

The permeability of the random packings is post-processed using Darcy's law, which describes the relationship of Darcy's flux (q) with the permeability (k) of a porous media. The law was initially formulated based on the results of experiments and has later been verified to be a homogenization of the Stokes formulation (Whitaker [50]).

$$k = \frac{\varphi v \mu}{\nabla p}$$

The flux of Dacry can be related to Stokes velocity of the fluid through the grains by multiplying with the porosity (φ). As the pressure gradient and dynamic viscosity is imposed in the model and we can measure the average velocity and permeability, which allows us to find the permeability of the samples.

2.2.3. Energy dissipation

In line with the homogenization scheme described in Section 2.1, the velocity of the fluid and the pressure gradient can be expressed in terms of the average value and the fluctuation (Whitaker [50]; Du and Ostoja-Starzewski [10]):

$$p = \overline{\nabla p} + \widetilde{\nabla p}$$

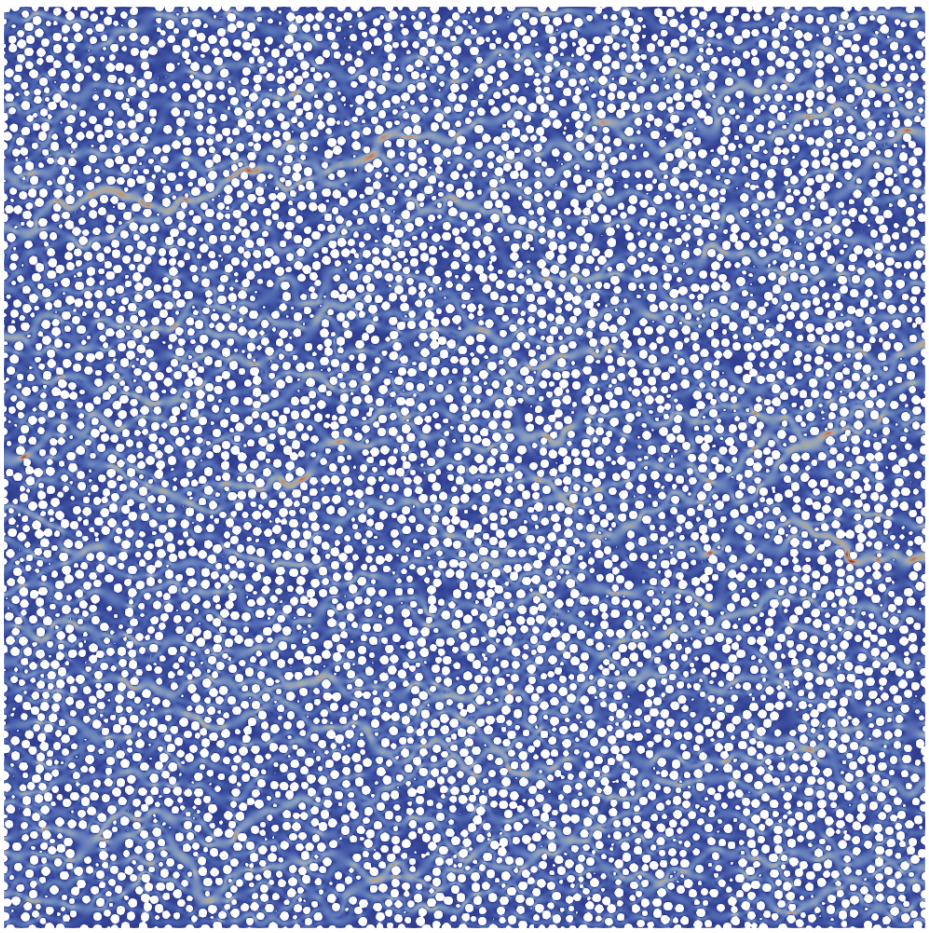

Figure 2.1: Example of flow through a random packing of spheres. The figure visualizes a cross-section, with a packing fraction of 32% of spheres with a diameter of 0.005 (compared to a total volume of 1). The grains are shown as white disks and the velocity of the fluid is shown in the coloured range, where blue is a low velocity and red is a high velocity.

$$v = \overline{v} + \widetilde{v}$$

The energy dissipation needed to study the evolution of the energy consistency is calculated by taking the product of the pressure gradient and the velocity of the fluid, which can also be described as an average value and a fluctuation term (Du and Ostoja-Starzewski [10]; Zhu et al. [52]; Paéz-García, Valdés-Parada, and Lasseux [33]):

$$E_{dis} = \overline{\nabla P v} = \overline{\nabla P}\,\overline{v} + \widetilde{\nabla P v}$$

The energy dissipation can only be post-processed over a volume when the fluctuation part is equal to zero, which is assured when the size of the sample is equal to a REV. In other words, once the energy of the fluid from the microscale becomes stable and matches the energy dissipation on the macroscale, the fluctuation of the energy is equal to zero. Conveniently, this means that the ratio of the energy is known to be unitary. We call this the energy ratio index.

$$\widetilde{\nabla P v} = 0 \quad \Leftrightarrow \quad \overline{\nabla P v} = \overline{\nabla P}\,\overline{v} \quad \Leftrightarrow \quad \frac{\overline{\nabla P}\,\overline{v}}{\overline{\nabla P v}} = 1$$

By combining the energy dissipation and Darcy's law, the permeability can be calculated with the energy.

$$k = \frac{-\mu E_{dis}}{\nabla p^2}$$

Thovert and Mourzenko [48] recommends taking an intrinsic volume away from the boundary into account to compute the effective properties. We, therefore, question whether it is possible to trace the evolution of the effective properties by gradually increasing the size of a sub-volume away from the boundaries, rather than simulating on increasingly larger volumes. This would drastically reduce the necessary computational resources, as the simulation for each random packing only needs to be performed once instead of for each step size. Furthermore, model properties, such as the boundary layer, only need to be determined once.

Since Thovert and Mourzenko [48] showed that the homogenized value within the intrinsic volume is the same, we expect the results of the different sample sizes to be the same. To validate this. we trace the evolution of the permeability of the same random packing, cut into different sizes with a constant step size of 5% in linear length. For each simulation, we calculate and trace the permeability within a growing subsample, as shown in Figure 2.2 for sizes ranging from 5% to 100%.

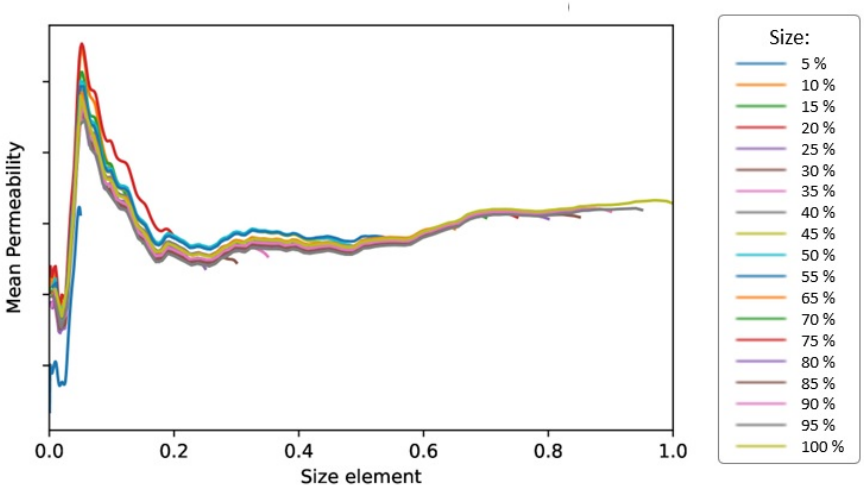

Figure 2.2: The mean permeability of a packing fraction of 32%, with a maximum sample size ranging from 5% to 100%. The permeability is traced by taking an increasing subsample up to the maximum range, starting at the centre of the sample.

We observe that the permeability of the different sample sizes evolves in a nearly identical matter, following the same values and trend. This confirms that it is possible to compute and trace the effective property, with a single simulation and by homogenizing the property over a growing sub-sample within the full sample. However, near the full simulation size of each different step size, a declining trend of the permeability is observed, diverging from the trend shown with bigger subvolumes. This can be explained by the influence of the boundary conditions.

2.2.4. Boundary effects

The extent of the boundary layer is determined, so that the postprocessing of the effective properties can be made without the influence of the boundary conditions. We determine the size of the layer by performing simulations with slip and no-slip boundary conditions on three samples. This allows us to analyse the difference in the properties between the models. To emphasize the boundary effect, the average of the mean energy inside the three different random packings is also plotted. This enables us to differentiate between the unique outcome of a single sample and a general trend regarding the packing fraction models. An example of the evolution of the energy is shown in Figure 2.3 for a packing fraction of 42%.

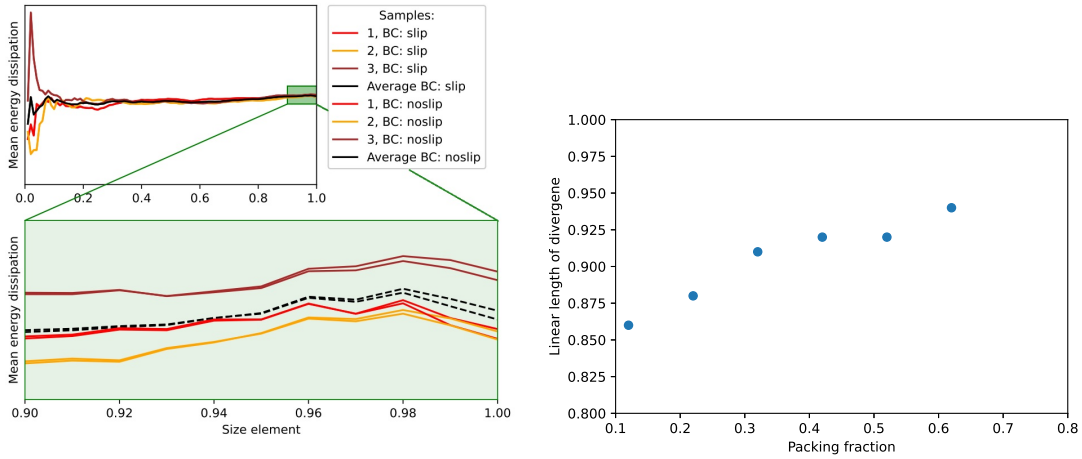

Figure 2.3: The boundary effects on the energy dissipation inside a random packing. An example of the divergence is shown on the left for a packing fraction of 42%. On the right, the maximum subsample, uninfluenced by the boundary conditions, is presented for the different Packing Fractions.

Packing Fraction	Mesh element size	Boundary layer
0.07 - 0.22	0.0004	15%
0.27 - 0.37	0.0004	10%
0.42 - 0.47	0.0001	10%
0.52	0.00009	10%
0.57 - 0.62	0.00008	5%

Table 2.1: The properties of the different models

The figure shows that the energy follows the same trend for all three different random packings, as a small increase of the energy appears in the last 8% of the full model after a stabilized value in the previous part of the graph. In the last 2% of the sample, a decrease in the energy is observed. The difference between the slip and no-slip external boundary conditions is also evident, as the values are identical up to the last 5% of the model and divergence from there on. The energy dissipation within the models of no-slip always presents a higher value than the slip conditions, which is because the no-slip boundary conditions force the fluid away from the external boundary. Therefore, we take the last ten per cent as the boundary layer which is influenced by the boundary condition. We find similar values for other packing fractions, with a boundary layer between 4% to 15%. For each packing fraction, the properties of the model set-up are presented in Table 2.1.

2.2.5. Mesh Convergence

Mesh convergence is a crucial aspect of numerical simulations, as it ensures that the solution obtained is independent of the discretization used and thus can be considered to be numerically accurate. When an increasing number of elements is applied in the mesh, we find that the value of the energy and permeability converges towards a unique value. We, therefore, normalise with regard to the last calculated value of the energy, as shown in Figure 2.4 for a random packing with a packing fraction of 32%. As the calculated result of the properties with half the amount of finite elements is within a 2% error of the normalised value, we assume the solution to be converged.

We observe that the size of the mesh elements is different for the different porosities. This difference in mesh elements is due to the mesh transition from representing the boundary of the grains to the void space within the random packing. The circular grains are challenging to represent using a triangular mesh configuration, which results in the need for more elements compared to the void space in between the grains. Consequently, higher packing fractions, which include more circles, require a smaller mesh element size. Note that the mesh convergence for the permeability is found earlier than for the energy.

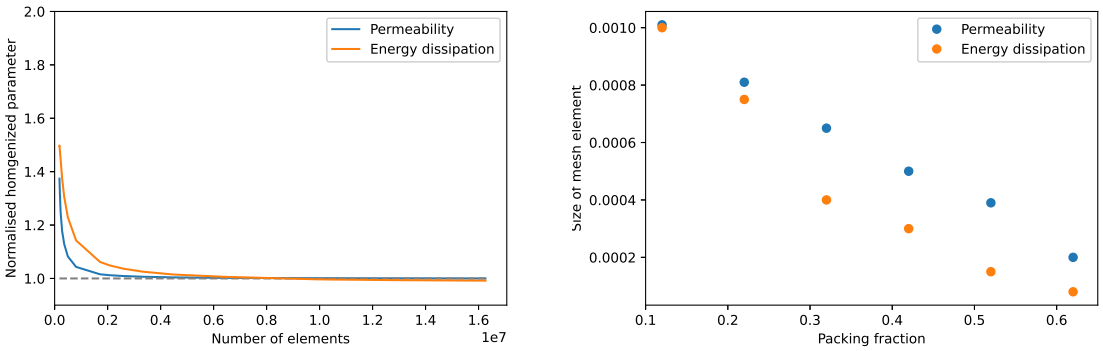

Figure 2.4: The mesh convergence of the normalised homogenized properties inside a 2D cross-section of a random packing. On the left, an example of the evolution of the mesh convergence is shown, for a packing fraction of 32%. On the right the values of the size of the mesh element are shown which correspond to the mesh convergence

2.2.6. Model verification

The Kozeny-Carman equation (Kozeny [21]; Carman [7]) is a relation to find the permeability of a bed with randomly packed spheres. The relationship was originally developed by Kozeny using the simplified model of parallel capillary tubes of equal length and diameter to describe a packed bed. Carman later calibrated the equation experimentally on real samples. The model assumes that the spheres have a uniform diameter and do not overlap. The flow of the fluid is assumed to be governed by Darcy's law, as the flow is laminar. The pores between the spheres are assumed narrow and any permeability of the solid grains is neglected. As these assumptions match our model rather well, the Kozeny-Carman model is used to validate our models.

The Kozeny-Carman model relates the permeability (k) with the sphericity of the particles in the packed bed (ϕ_s), the porosity of the sample (ϕ), the average diameter of the grains (D_p) and the Kozeny constant (K), depending on the tortuosity of the sample:

$$k = \phi_s^2 \frac{\varphi^3 D_p^2}{36K(1-\varphi)^2}$$

The results of the numerical method and Kozeny-Carman model are compared and shown in Figure 2.5. We observe that the outcome of the mean permeability is very similar, in both values and trends with the porosity. At lower packing fractions the assumption of narrow pore spaces is no longer valid and at higher packing fractions the complexity of geometry, with overlapping grains, and flow path may not be accurately captured by the Kozeny-Carman model, which is observed by the divergence of both models near the tail-ends of the considered porosities. Similar results have been found in other research studies (Cancelliere et al. [6]; Lesueur et al. [24]). Therefore, we conclude the model setup is correct.

2.2.7. Results

The energy of the fluid is traced, starting from the middle up to the edges of the maximum subsample, for each sample. Figure 2.6 displays the evolution of the energy ratio, macro to micro scale, for different porosities. For each porosity, 100 Monte Carlo realizations have been computed, as shown in grey. To present the overall evolution of the energy ratio, the average of the mean energy is plotted in blue.

We observe that the energy ratio for each microstructure evolves with a unique trajectory, varying and oscillating in values, especially considering smaller volumes, which indicates that energy consistency does not exist at this stage. However, the energy ratio of every microstructure eventually converges towards a stable value of one. All microstructures together show a cone-shaped convergence towards an energy ratio of one with a decreasing variation of the energy ratio with growing subsamples. The small variation of the energy ratio, together with the stable value of one, indicates that we have found

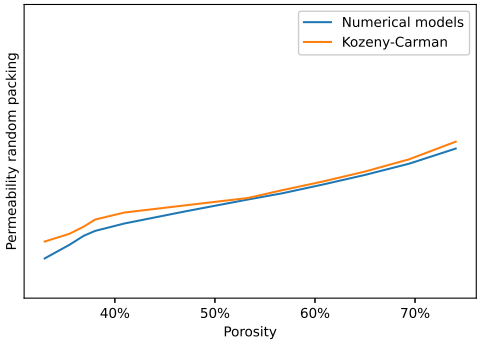

Figure 2.5: The comparison of permeability of packing fractions, computed with the Kozeny-Carman (orange) and the numerical models (blue)

energy consistency across the scales, and therefore have found the REV. The average value quickly converges towards one, after a higher value in the beginning, which shows that value is truly converged. The high value of the mean average energy ratio in the beginning can be explained by the big spread of the energy ratio, which does not drop below zero but includes higher values.

Higher porosities display a slower convergence than lower porosities. For example, the variance of the energy ratio for a microstructure with a porosity of 69% is lower than 0.25 around 20 times the length of the sample diameter of the grain ratio (L/D) and drops below 0.1 around 50 L/D. Whereas a porosity of 47% has a variance lower than 0.25 near 10 L/D, drops below a variance of 0.1 around 25 L/D and is neglectable after 40 L/D.

As we observe a converged unitary value of the energy ratio for all models, including a clear rapid convergence, we show that the energy consistency is found within the intrinsic sub-sample. This means that the requisite of the energy conservation prescribed by the Hill-Mandel principle is only met at a certain volume, which is the REV. Current homogenization schemes already require the REV for valid homogenization, so eventually, we fall back to the same constraints, albeit with a known converged value. Therefore, homogenization can be applied utilizing the known unitary effective energy ratio and unaffected by upper or lower bound estimations.

2.3. Application to real microstructures

Section 2.2 showed the theoretical behaviour of the conservation of the kinematic flow energy in idealized microstructures. Using random packings with spheres, we showed that we find energy consistency within an intrinsic subsample, unaffected by the boundary conditions. Therefore, we showed that we can apply homogenization, without the enforcement of the boundary conditions. We now verify this outcome by tracing the energy ratio within real microstructures, which include natural heterogeneities, possibly affecting the results.

The process of digital rock reconstruction follows the framework of Lesueur et al. [24]. Segmented 2D micro CT scans are translated to 3D computational models, in which the rock and void space are separated. In order to reduce the computational costs of the simulations, we use the Displaced Boundary method Lesueur, Rattez, and Colomés [23] to conform the pore-boundary interface to a coarser background mesh. It is shown that mesh convergence is still achieved with a coarser mesh, which results in the reduction of computational costs of the simulations. The mesh structures are used to apply the flow simulations.

While random packings are generated with an algorithm and an unlimited number of microstructures can be created, the structures obtained from CT scanning are limited by the sample size and scan resolution. Tracing the energy ratio throughout the full sample will provide a single curve and therefore is not statistically representative. To provide an overview of the variation of the energy dissipation within the

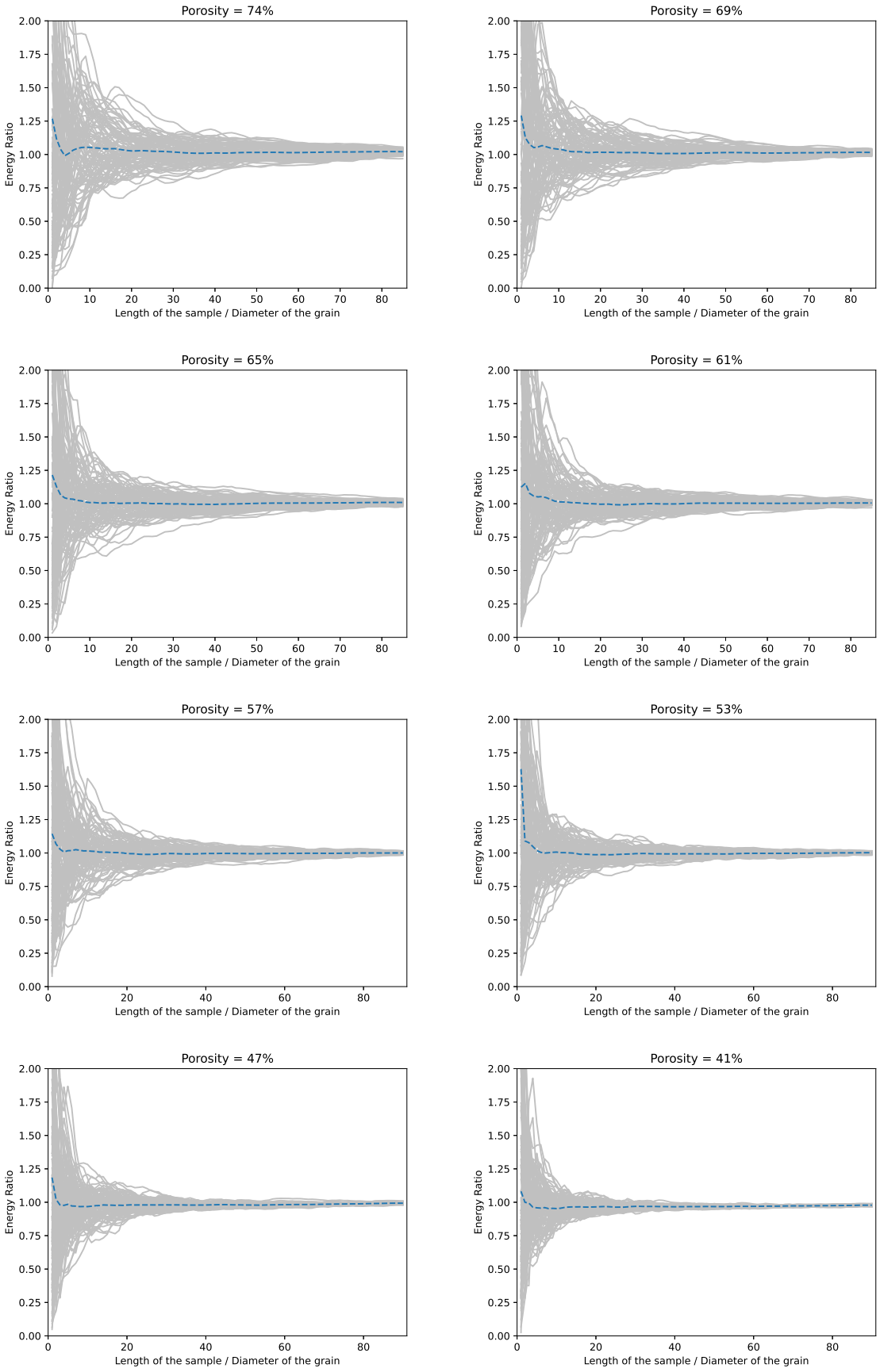

Figure 2.6: Energy consistency ratio evolution for different porosities, on a scale of length/ diameter ratio. Each grey line is a new random packing, and the blue line represents the average energy ratio of all the random packings at the considered length.

full rock sample, the sample is divided into multiple subsamples. The size of the subsamples is bigger than the average grain size to ensure they accurately reflect the behaviour of the fluid energy inside the rock. To achieve this, the sample is divided into 4^3 equal-sized subsamples. Splitting it into fewer subsamples would result in a bigger subsample size, yet less statistical representativeness of the energy ratio. Splitting it into more subsamples would result in a very small maximum size of the samples, which might not be reflective of the real rock sample. The subsamples do not overlap and therefore the independence of the energy dissipation is ensured for each subsample, as it is not affected by the other subsamples. Like the whole rock, the development of the energy ratio inside the sub-volumes is traced with an intrinsic volume which is independent of the boundary conditions, growing from the centre up to the edges.

The first microstructure is the LV60A [38] sand pack, shown in Figure 2.7a. Sand packs are monomineralic, which makes them quite homogeneous in both grain size and shape, yet include natural heterogeneities such as the grain roughness and non-sphericity of the grains. Sandpacks also show high permeability, as the voids within the sample are connected throughout. The LV60A is characterized by a porosity of 68% and a characteristic length of 149 μm. The influence of the occurring natural heterogeneities on the energy dissipation is expected to be low, considering the fairly homogeneous characteristics of the sand pack. Therefore, this is deemed to be an excellent start to verify the previously found results with the random packings. The LV60A sand pack has a full size of just above three mm and with a scan resolution of 10.008 μm, the result of the rock reconstruction is 300^3 voxels.

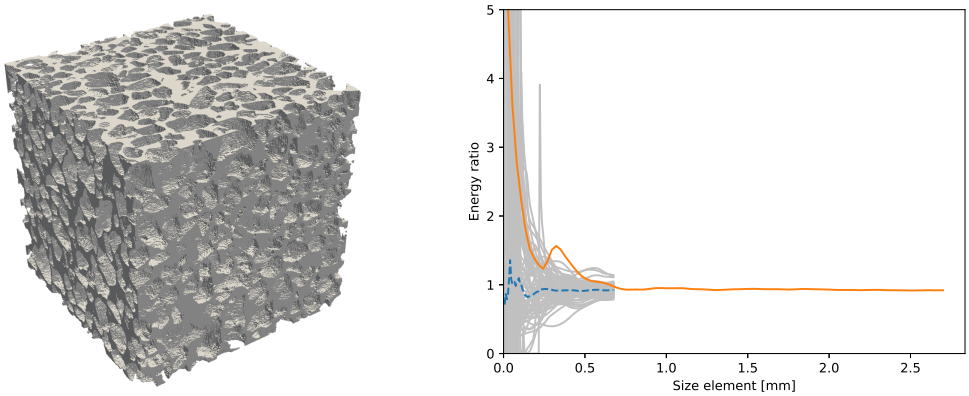

Figure 2.7: On the left a reconstruction of the LV60A sand pack pore space is displayed. On the right, the tracing of the energy ratio index of the sand pack is shown. The mean energy in the 64 sub-volumes is shown with grey lines and the average of the mean energy in the blue dashed line. The energy in the full sample is shown in orange.

We observe that the sand pack shows a convergence in the shape of a cone towards a value of one, similar as found while analysing the random packings. The energy ratio index inside the subsamples, plotted in grey, displays a high variation of the energy index, as the ratio reaches values above five, considering a linear length up to 0.2 mm. We also observe parts of the sample without any fluid energy in that region, distinguished with an energy ratio of 0, which were not noticed with regard to the random packings. The energy ratio index shows a rather fast convergence, as the variance at 0.7 mm is equal to 19%. This convergence is emphasized by the average of the energy ratio of the fluids inside the subsamples, plotted in blue, which shows a stabilizing trend towards one after 0.2 mm. The full sample, plotted in orange, starts at a high energy ratio above five and follows the rather smooth convergence towards one. As we observe a stabilized trend in the energy ratio index of the full sample and a low variation of the index within the subsamples, we conclude that we have found energy consistency throughout the scales. This means it is possible to apply valid homogenization at REV, at one mm in linear length. A similar trend and size of the REV can be observed in the study of Mostaghimi, Blunt, and Bijeljic [31], which finds a REV of 1.1 mm in linear length.

The second sample is the S1 sandstone Pore-scale Imaging and Modelling [39], shown in Figure 2.8a.

Whereas sand packs are typically made of individual grains, sandstone is a rock with a much more cohesive structure where the grains are cemented together by minerals. Sandstones often have lower permeability, as the voids show a lower connectivity and flow paths are more tortuous than sand packs. The S1 sandstone is characterized by a porosity of 20% and a characteristic length of 311 μm. All of this results in slightly more heterogeneous properties overall. With a scan resolution of 8.7 μm and a total sample length of 2.6 mm, the S1 sandstone image contains 300^3 voxels.

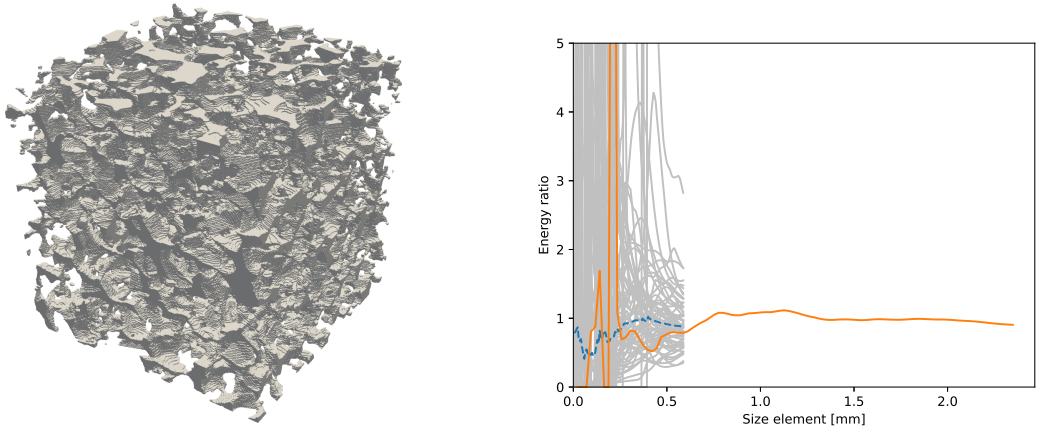

Figure 2.8: On the left a reconstruction of the S1 sandstone pore space is displayed. On the right, the tracing of the energy ratio index of the sandstone is shown. The mean energy in the 64 sub-volumes is shown with grey lines and the average of the mean energy in the blue dashed line. The energy in the full sample is shown in orange.

The results of the S1 sandstone are plotted in Figure 2.8b. As expected, the energy ratio index is more scattered within the subsamples of the sandstone, as shown in grey. The energy ratio shows values of zero up to five within a region of 0.4 mm. To put it into contrast, this region was only half as big when the sand pack was analysed. From 0.25 mm, the energy index inside the sandstone also shows a cone-shaped convergence towards a value of one, like the sand pack and the random packings. Although, at the maximum size of the subsamples (0.54 mm), the maximum variation of the index still has a value of 0.6. Tracing the energy ratio index of the full sandstone sample, plotted in orange, presents a similar trend. The values of the energy ratio oscillate quite heavily at the beginning of the figure but stabilize around a value of one at a linear length of 0.6 mm. A completely stable line, which was observed with the sand pack, is not found, since the value of the energy ratio still slightly decreases. This means REV has not fully been reached yet. Although, with an energy ratio value near one (0.93) and the decreasing variance of the index, it is logical to assume we are close to the REV. Similar trends are shown in Mostaghimi, Blunt, and Bijeljic [31], tracing the permeability of the sandstone. The variance of the permeability dampens out, but the traced average permeability of the full sample still presents a decreasing trend when the full sample of the sandstone is considered.

The third sample is the Ketton limestone [30], shown in figure 2.9a. Limestone is mainly composed of calcium carbonate and therefore usually quite heterogeneous. The grain shape and sizes vary substantially and the pore spaces may not always be connected. This Ketton sample is rather homogeneous for a limestone and has voids reasonably well connected. The Ketton limestone is characterized by a porosity of 13% and a characteristic length of 331 μm. Where many similar rocks do not reach the REV when the full sample is considered, we expect this to be different with the Ketton rock sample. The sample with a size just over three mm has a much higher CT-scan image resolution compared to the others, of three μm, resulting in a digitised microstructure with 1000^3 voxels.

The results for the Ketton are plotted in Figure 2.9b. As we observe the variation of the energy ratio of the Limestone, we find very similar trends as shown in the results of the S1 Sandstone. The energy ratio of the subsamples of the Ketton Limestone, plotted in grey, include values from zero and over five of the energy ratio up to a linear length of 0.4 mm, which matches the results of the sandstone. The range of the energy ratio value decreases in the region above 0.4 mm, as we find a variance of

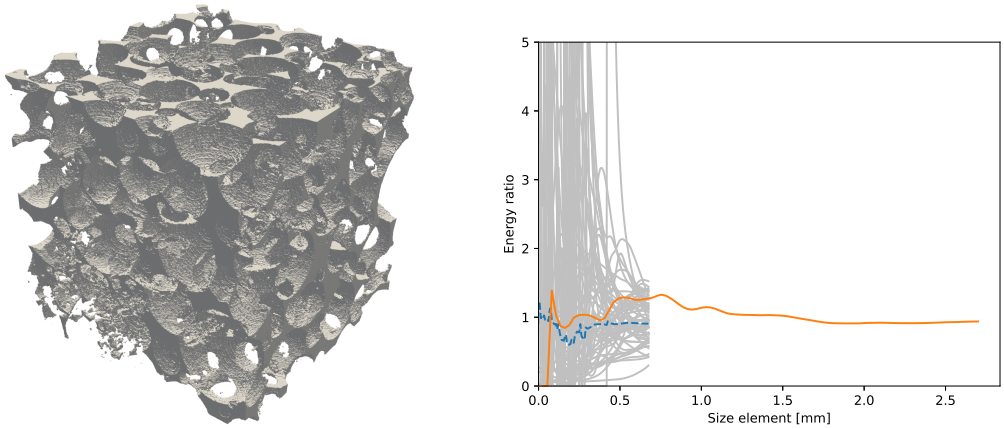

Figure 2.9: On the left a reconstruction of the Ketton limestone pore space is displayed. On the right, the tracing of the energy ratio index of the limestone is shown. The mean energy in the 64 sub-volumes is shown with grey lines and the average of the mean energy in the blue dashed line. The energy in the full sample is shown in orange.

the energy ratio of 0.5 around 0.7, which is also similar to the sandstone. The average energy ratio of subsamples, plotted in blue, oscillates noticeably until the maximum values of the energy ratio drop below five, which is also similar to previously found results. Above 0.4 mm, we observe a stabilizing trend of the average energy ratio, convergence towards a value close to one. The full sample reaches a stable value of the energy ratio around one after two mm in length, after an osculating up to 0.5 mm. Together with the low variance of the subsamples near 0.6 mm, the flow energy can be considered to be converged at a value of one at two mm, and therefore energy consistency is found naturally.

The last sample is the C2 carbonate Pore-scale Imaging and Modelling [37], shown in Figure 2.10a. The C2 carbonate exhibits a high heterogeneity in grain properties and low connectivity of the voids, which results in a low permeability overall. The C2 carbonate is characterized by a porosity of 14% and a characteristic length of 220 μm. [31] has shown that the size of the REV is not found for the permeability, even when the full sample is taken into account. The sample has an image resolution of 5.7 μm and with the total size of the sample of 2.3 mm, the result is 400^3 voxels.

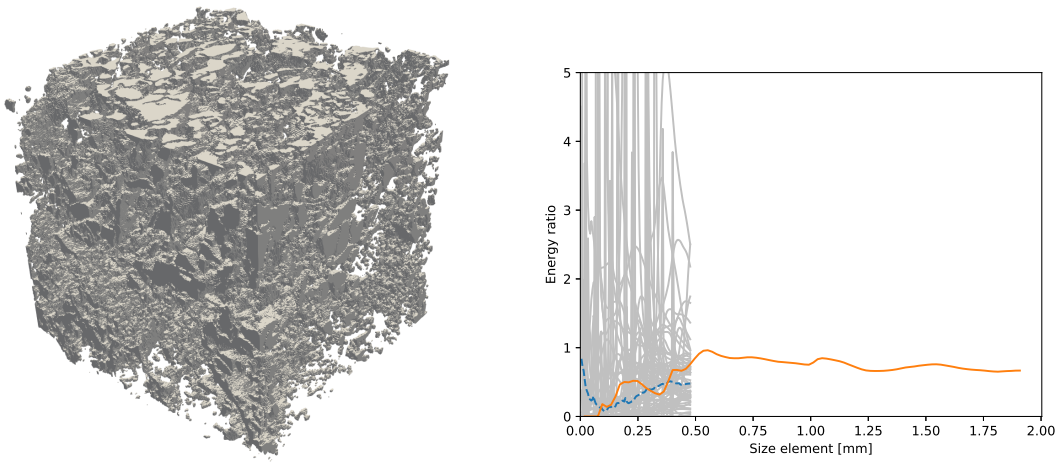

Figure 2.10: On the left a reconstruction of the C2 carbonate pore space is displayed. On the right, the tracing of energy ratio index of the carbonate is shown. The mean energy in the 64 sub-volumes is shown with grey lines and the average of the mean energy in the blue dashed line. The energy in the full sample is shown in orange.

The results for the C2 carbonate are shown in Figure 2.10b. The subsamples show a huge variance in the energy ratio index, compared to the previously assessed rock samples. Whereas we find values of

the index from zero and above five until 0.4 mm in the Ketton and S1, the C2 exhibits these values up to 0.5 mm, which is the maximum size of the subsamples. The average value of the energy ratio of the subsamples, shown in blue, oscillates as well and does not necessarily seem to go to one. However, tracing the energy ratio index of the full sample, plotted in orange, appears to be more stable. The values vary considerably within the region of the subsamples but seem to stabilize towards a value of 0.85 afterwards. The varying values of the index in the subsamples and the not fully converged value of the full sample indicate that we have not reached REV yet, or might not even be close. The previously assessed rock samples show a clear trend of convergence after the percolation threshold has been reached, whereas this C2 carbonate lacks this convergence and still contains values below the percolation threshold at the full length of the subsamples. This makes it impossible to conclude whether or not the energy ratio will converge towards a value of one. Thus we cannot utilize the energy consistency and apply valid homogenization for the C2 carbonate.

2.4. Conclusion

In this contribution, the Hill-Mandel principle of energy conservation throughout the transition of scales is revisited. This requirement for rigorous homogenization is usually enforced by applying specific boundary conditions, which however influences the resulting effective properties, in both magnitude and rotation.

Using results of simulations of Stokes-flow through digitised microstructures, this study assesses the consistency of the energy of fluid inside idealized microstructures, random packings of spheres, inside an intrinsic volume, away from the boundary layer and therefore uninfluenced by the boundary conditions. This energy consistency is found inside the intrinsic volume when the energy ratio of the micro- and macro-scale goes to one. In that case, the requisite of energy conservation of the Hill-Mandel principle is met and homogenization can be applied. This intrinsic value will capture the true value of the effective property instead of an upper or lower bound estimation, obtained due to boundary conditions.

The energy ratio index of the increasing idealized microstructure follows a cone of convergence, which always reaches one, despite the consideration of different porosities. Whereas traditional homogenization schemes use an iterative process to determine the stabilized property value, which is usually unknown, the energy ratio index converges to one and therefore provides a more accurate indicator of REV convergence.

We extend the results of the random packings to real rock microstructures, which include natural heterogeneities. We show that those heterogeneities mainly influence the width of the base of the cone of convergence, as the variance at the base is a lot higher than for the random packings. Still, the cone converges towards an energy ratio of one, which means the Hill-Mandel principle is eventually respected. Despite a slower convergence, the heterogeneities of natural rocks do not influence the principle of energy conservation and it remains possible to apply valid homogenization at REV, even when are heterogeneities present.

We note that the size of the convergence of the energy ratio inside real microstructures seems to directly depend on the percolation threshold. The energy ratio fluctuates considerably when sub-samples are not percolating. This is observed with highly heterogeneous samples and this behaviour prevents an accurate approximation of the REV. In comparison, when the percolation threshold is reached, the mean value of the energy ratio stabilizes and reaches convergence quickly.

3

Predicting the REV by determining the evolution law of the cone of convergence

Abstract

To find the effective physical property of a rock, it is required to find a volume for which the homogenised property does not fluctuate when the size of the sample is increased; the Representative Elementary Volume (REV). Its determination usually comes at the cost of a large number of simulations, making it overall a computationally expensive process. Therefore, many scientific studies have been dedicated to optimize the process of finding REV. Using statistical numerical methods, it is shown that the fluctuation of the effective property corresponds overall to a cone-like shape convergence. We suggest determining the generic evolution law of the cone of convergence, which can be used to predict the size of the REV and the effective physical property.

This study is based on simulations of Stokes flow through idealised microstructures from which the permeability is upscaled. By tracing and plotting the convergence of permeability for multiple samples, the full cone of convergence appears. The cone shows exponential growth and decay, converging towards the effective permeability of the microstructure. By fitting the log-normal distribution on the collected data points, we can describe the generic evolution law of the cone of convergence. This accurately describes the base of the cone, despite the different porosities. The evolution of the cone is described with an exponential function, using the reference variance and mean of a log-normal distribution as input.

We show that the determined law of the cone also applies to real microstructures, despite the presence of natural heterogeneities. The importance of this contribution is that we eventually show that it is not necessary to simulate the full sample to find the REV, which is computationally expensive, but instead, a number of small subsamples, depended on a predetermined accuracy, is sufficient to predict the size of the REV and the effective property when the convergence law is known.

Keywords

Representative Elementary Volume, Convergence Cone, Permeability

3.1. Introduction

To understand the behaviour of rock media and their properties, it is essential to study the microscopic scale. For example, the porosity, connectivity of the voids and other morphologic parameters of rock media will determine the overall permeability of the material (D. C. Beard [9]; Cox and Budhu [8]; Torskaya et al. [49]). However, modelling larger structures using microstructures is not practical, as it

requires high computational power to capture the microscopic complexity. Digital Rock Physics (DRP) provide a scheme to upscale the physical of the heterogeneous porous media to the macroscopic scale.

The upscaling of the physical properties from the microstructures to the macroscale requires the determination of Representative Elementary Volumes (REV). These are the smallest volumes of a heterogeneous sample that can accurately represent the mean constitutive response at the macroscopic scale. In DRP defining the REV is crucial as the physical properties of the porous media can vary significantly when microscopic scales are taken into account. This makes it difficult to model and predict the behaviour of the rock sample on a larger scale, based on microscopic samples. By identifying and characterizing the REV, the physical quantities can be upscaled from the microstructure and used for macroscale applications. Another benefit of REVs is the ability to apply multiscale modelling. The homogenized macroscopic response is used as input to the microscopic boundary value problem, which in turn provides the material response at the macroscale. This circular system allows for the determination of non-physical responses in the overall material behaviour without making any assumptions.

The determination is a fundamental exercise in DRP, yet it remains a challenging task due to the complex nature of these porous media. The physical properties of the microscopic samples are measured and homogenized on a growing subsample. As smaller volumes of the porous medium can exhibit significant variances in the properties, larger volumes are needed to achieve convergence to a stable value. However, tracing this convergence is computationally expensive as multiple simulations are needed with a growing sample size to obtain an accurate measurement of the physical property. Especially the larger volumes can be computationally demanding, in both resources and time.

Therefore, researchers have tried to simplify and optimize the process of finding REV. Some studies have shown that the REV can be related to the size of the grain, studying a specific physical property and the morphology of the microstructure. Elvin [11] showed that the number of grains required for homogeneous elastic behaviour of polycrystalline should be at least 230. Ren and Zheng [42] tested over 500 cubic polycrystals in the plane stress problem and showed that the REV size of the polycrystals is roughly 16 times the grain size. Liu [25] determined experimentally that the minimum size to represent uniaxial compression and thermal expansion of PBS 9501 heterogeneous materials with an average crystal diameter of around 100 μm is approximately 1.5 mm. Grimal et al. [17] studied bone biomechanical behaviour and showed that the REV size of the elastic coefficients of the tissue is about 1.5 mm. There are many more examples of studies using different physical properties in combination with different materials, showing a specific size as a REV. However, if the input parameters, such as the type of material or physical quantity being assessed, are changed, the size of the REV will change.

In order to find a more generic way of finding REV, not necessarily depending on a specific property or type of material, other studies have provided methodologies. Shan and Gokhale [46] developed a methodology involving the use of stereological and image analysis techniques to quantitatively characterize the microstructure of ceramic matrix composites. This is used to create a computer-generated REV which is statistically representative of the real microstructure, including fibre-rich and -poor regions. Sebsadji and Chouicha [45] used a representative unit cell approach, assuming a unit cell to be periodic over a specific sample in order to find the REV, which is characterized by a power-law particle size distribution. While these methodologies provide useful approaches for finding the REV in different materials and media, they are still time-consuming and require significant computational power.

To get more insight into the evolution of the convergence, numerical-statistical methods have been applied in the process of finding REV. Graham and Yang [16] studied the geometrical properties of the microstructure and show that the variance of the particle distribution within the sample converges with an increasing measured area. Du and Ostoja-Starzewski [10] presented the rate of convergence based on the number of grains in a length, depending on the porosity, with a decreasing variance of the porosity considering larger samples. Łydżba and Różański [26] studied the heat flow and the linear elasticity of a random media. They applied a two-point probability and a lineal-path function to find a converged value of the physical properties. Kanit et al. [20] presented the REV for linear elastic properties and thermal conductivity including a convergence of the variance considering larger samples. Kanit shows that the properties can be determined not only using numerical simulations on large volumes but also

with mean values of multiple small volumes. Pelissou et al. [34] continues the work of Kanit, using a new stopping criteria to reduce computational costs, which is especially convenient in non-linear cases. Mirkhalaf, Pires, and Simoes [29] utilizes the statistical-numerical approach to find the REV for polymers subjected to finite deformations with a predefined percentage of the average deformation and a predefined error as the stopping criteria. Rahman et al. [41] showed the convergence for porosity for five different rock samples and also demonstrated that the variance of the porosity can be used as a qualitative indicator for rock heterogeneity.

The numerical-statistical studies clearly show that the process of finding the REV results in a cone-shaped convergence of the physical property. The property varies sustainably when different smaller volumes are considered. As the size of the samples is growing, the variance of the property will decrease and converge towards a stable value. When the variance of the property is small and the average value of the property has stabilized, the size of the REV can be determined. Due to the direct correlation between the geometric properties of the microstructure and the homogenized physical quantity, the convergence is always bounded by the cone shape, starting with a large width and becoming increasingly narrow with a growing sample size.

In this study, we propose a new method to find REV, utilizing the known shape of the cone of convergence. The shape provides both information on the rate of convergence and the homogenized property, allowing to find the REV in a more efficient and accurate way. In addition, if the digital rock sample is not large enough to find REV, which is often the case considering carbonate rock samples, the cone of convergence can still provide information about the size of the REV and homogenized property. With a focus on permeability, a property of significant interest in DRP, we aim to find the evolution law of the cone of convergence. The energy dissipation will also be considered due to its relevance to homogenisation schemes Zwarts and Lesueur [53].

This paper is organized as follows: In section 3.2, we introduce and determine the generic evolution law of the cone of convergence with idealized microstructures. In Section 3.3, the generic evolution law is applied to real microstructures, to validate whether or not the generic evolution law still holds when natural heterogeneities interfere. In Section 3.4, the requirements to fit an accurate cone of convergence are discussed and compared to traditional methods.

3.2. Material and methods

As described in the introduction, the properties of the grains are known the be a big influence on the permeability of a rock sample. This study aims to find the generic evolution law of the cone of convergence, hence we avoid considering the influence of the grain properties on the permeability and the energy dissipation by considering an ideal porous medium, random packings of perfectly round spheres.

The method applied to generate and mesh the random packings, the Stokes-flow model and post-processing of the permeability and energy dissipation are shown in Zwarts and Lesueur [53]. The random packings are generated and with Finite Element simulations of Stokes-flow, we can calculate the energy dissipation and the permeability of the samples. With the recommendations of Thovert and Mourzenko [48] in mind, the postprocessing of the effective properties will be applied within a subvolume, without the influence of the boundary conditions. We follow the recommendations from Zwarts and Lesueur [53] and plot the evolution of the energy dissipation ratio index across the scales to determine the REV of the permeability. At REV, we respect the Hill-Mandel principle and obtain therefore the energy consistency across scales, which means that the ratio becomes unitary.

3.2.1. Generating the cone of convergence

The cone of convergence appearing on a REV convergence graph, shortened to convergence cone or cone of convergence in this article, represents the convergence of homogenized properties for samples with increasing size. The cone consists of a collection of data points, each representing the value of a homogenized property obtained from different samples that vary in size and geometrical properties of the microstructure. Due to the substantial variability of the homogenized properties for small samples

and then the convergence with increasing sample sizes, this cone shape naturally appears.

In this research, the data points are obtained by tracing the permeability and energy dissipation for a series of random packings with the same characteristics. For each sample, the properties are traced with the help of a growing subsample, starting from the centre of the random packing, and gradually growing to the maximum size of the sample. This way, we can trace and plot the evolution of the properties for a single sample. We repeat the process of tracing the parameters for a series of samples and plot it all together in the same graph, Figure 3.1, where we can see the cone shape appearing. To analyse the behaviour of the cone of convergence, we consider 100 samples for each packing fraction, ranging from 0.07 up to 0.62. This number of models allows us to visually display the cone of convergence and is verified later to be statistically representative of the accurate description of the cone.

3.2.2. Evolution law of the cone of convergence

The shape of the cone of convergence is visualized with a grey colour through the superposition of the trace of the individual samples, shown in Figure 3.1. We present the convergence for the permeability in the left column and the energy dissipation ratio on the right. Each row of figures presents the REV convergence for a different porosity, which was controlled by the packing fraction. The data for the energy dissipation ratio index is taken from Zwarts and Lesueur [53].

All the cones start with a large base at small sample sizes and converge towards a certain value, as shown by the decreasing width of the cone. The energy ratio, in particular, converges towards a value of one. Note that the missing spaces present in the cone would be filled if more statistical representativeness is considered. The mean value of all the samples of the homogenized properties is plotted with a dashed blue line. Compared to the overall convergence of the cone, we observe a faster convergence of the mean value, which stabilised value is the true effective homogenized property.

From a statistical point of view, the boundary (y) of the cone at each size (s) can be described with a positive or negative standard deviation (σ) from the mean value (μ), as shown in Equation 3.1.

$$y_s = \mu_s \pm \sigma \tag{3.1}$$

We notice that the cone is not exactly symmetric around the mean value, as the top part of the cone presents a steeper convergence than the lower part. This means that the standard deviation used in the description of the cone has to be asymmetrical.

Upon closer inspection of the small sizes, we observe that the energy dissipation ratio index and the permeability vary with a range between zero and very high values. The range is realistic because at the microscale the flow can vary between being completely blocked by the grains of the rock or having a completely unobstructed flow path. This corresponds to respectively zero permeability and a high value, and similarly for the energy dissipation, as shown in Zwarts and Lesueur [53]. We also observe that the distribution of the data points is not exactly symmetric around the mean value, shown in Figure 3.2. Most values fall between zero and two, and only a few go up to higher values. The distributions at bigger sizes, also shown in Figure 3.2, present a smaller range of values, centred around the energy ratio of one. In addition, the histogram is becoming more symmetric around one.

The general shape of the cone and the shape of the histogram of the small samples seems to follow the shape of a log-normal distribution. The log-normal distribution has an asymmetrical range between zero and infinity, which therefore includes the very high values observed at the beginning of the cone. We note that as the variance of a log-normal distribution becomes small, the difference with a normal distribution becomes small. This means that the increasingly symmetrical shape with bigger sample sizes can still be accurately described by a log-normal distribution. Therefore, we fit a log-normal distribution over the collection of our data points of the REV convergence and describe each distribution at every size within the log-normal space.

$$\ln y_s = \langle \ln \mu_s \rangle \pm \sigma_{ln;s} \tag{3.2}$$

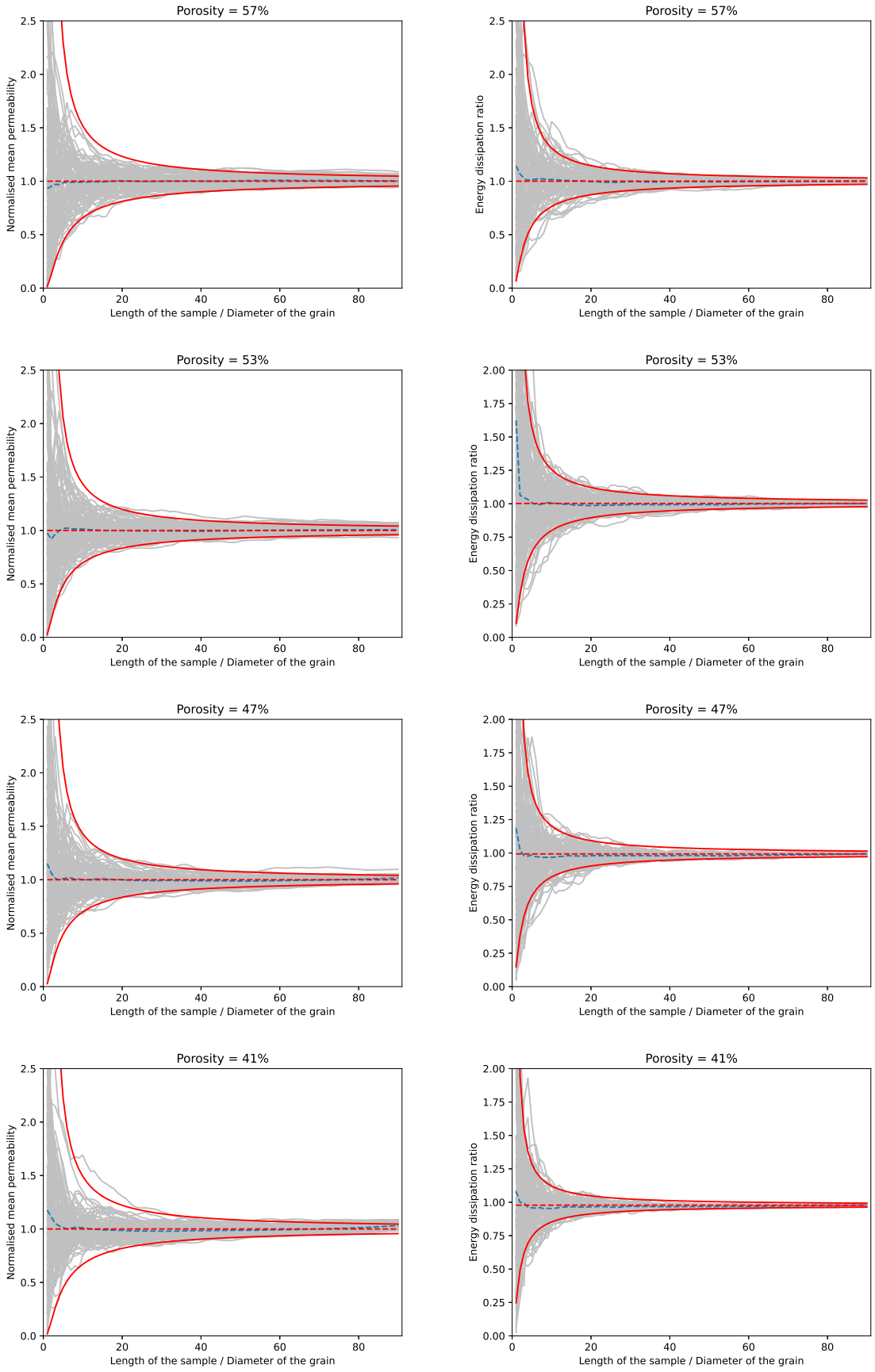

Figure 3.1: This figure presents the different cones of convergence varying in porosities and physical properties. The left column displays the evolution of the normalised permeability of various porosities and the right side shows the development of the energy ratio. The grey lines show the evolution of the individual random packings and the blue dashed line presents the average value of the mean properties. The red lines are the determined evolution law of the cone of convergence, with the mean value plotted in a dashed line and the boundaries as the continuous line.

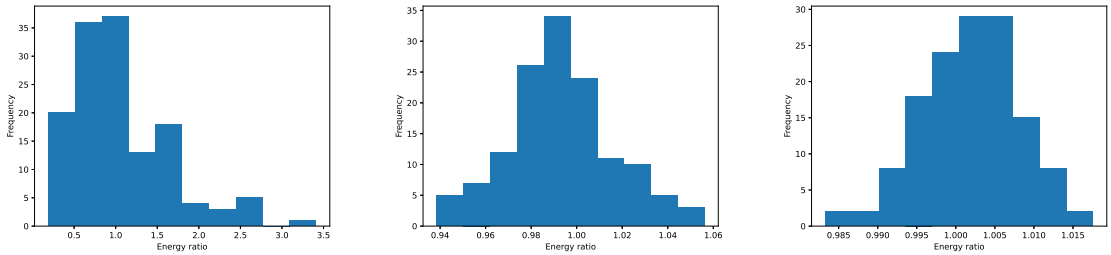

Figure 3.2: Histograms of the energy dissipation ratio index with a minimum, half and maximum subsample size of the samples with a packing fraction of 32%.

For simplicity, we will refer to the log-normal standard deviation of the distribution $\sigma_{ln;s}$ with σ_s from here on. The permeability and the energy dissipation are intrinsic average properties of the rock sample. Thus, we are looking for a way to describe the distribution in terms of the mean and the variance of the mean. The geometric mean value of the cone is clearly consistent throughout the evolution of the cone, except with very small samples. This is because the range of the values is quite large with small samples, which increases the standard error of the sample (Altman and Bland [1]).

As the corresponding sample size of the observations (n) of the cone grows with the evolution of the cone of convergence, the bigger samples include the smaller sample sizes. Therefore, we assume that the mean value of a larger sample with a certain size (V_s) is equivalent to the average of the means of the amount of smaller samples which fit in the larger sample. We consider this by introducing a reference sample (V_{ref}). The size of the reference sample is determined by the user of the cone and the bigger samples include a number of reference samples.

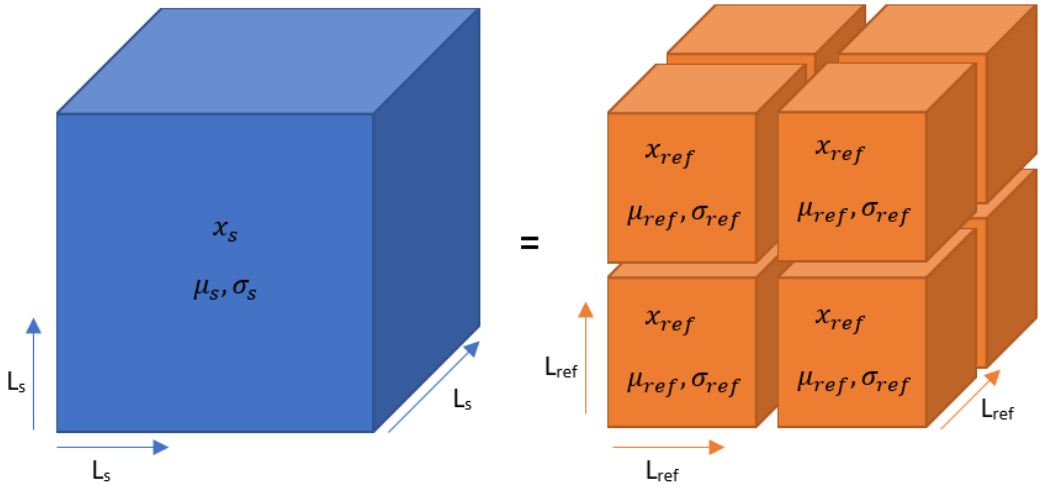

Figure 3.3: The principle of the mean value of a larger volume, which is equal to the mean of the means of smaller (reference) volumes

The value of the geometric mean value (μ) is approximated with a weighted average $(\langle x \rangle)$, proportional to the sample size (V_i), similar to what is shown in Figure 3.3.

$$\ln \mu \approx \langle \ln x \rangle = \frac{\sum_i^n \ln x_i \cdot V_i}{\sum_i^n V_i} \tag{3.3}$$

For the determination of the variance, we fall back on the law of large numbers and the variance-of-

the-sum rule, that describes that the variance of a mean from a number of independent observations of the same distribution is calculated by taking the average of the variance-of-the-sum. We apply this principle on the variance of a sample with a certain size (σ_s^2) and add the number (N) of reference samples which fit in the bigger sample, as shown in Equation 3.4. The number of reference samples is equal to the ratio of the sample size with the reference size.

$$\sigma_s^2 = \frac{1}{N^2}\sum_{i=1}^{N}\sigma_{ref}^2 = \frac{N\sigma_{ref}^2}{N^2} = \frac{1}{N}\sigma_{ref}^2 = \frac{1}{V_s/V_{ref}}\sigma_{ref}^2 = \frac{V_{ref}}{V_s}\sigma_{ref}^2 \tag{3.4}$$

To ensure that the observations are independent, we advise to only consider the bigger samples, as tracing the samples would make the observations of the effective properties dependent on each other and the bigger samples include the mean values of the smaller samples. With the log-normal distribution and observations of a certain size (n_s) included, the reference variance is calculated with Equation 3.5.

$$\sigma_{ref}^2 = \frac{V_s}{V_{ref}}\sigma_s^2 \approx \frac{V_s}{V_{ref}}\frac{1}{n_s}\sum_{i=1}^{n_s}\left(\ln\frac{x_i}{\mu}\right)^2 \tag{3.5}$$

We verify the principle of the means and the applicability to describe the evolution of the variance with a reference value. Figure 3.4 shows the difference between the variance calculated at each subsample length and the determined relation of the variance with the reference value, shown in Equation 3.4. We obtain the same values with both methods and can therefore conclude that the mean values of bigger samples are indeed correlated to the mean values of smaller samples and can be directly related to a reference variance.

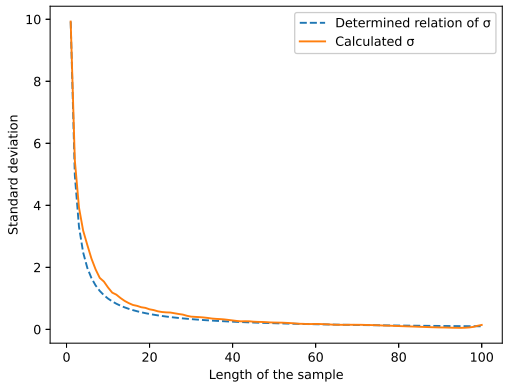

Figure 3.4: Evolution of the variance according to the size of the model. The orange line is the standard deviation computed per sample size and the blue dashed line is the standard deviation in relation to the reference value.

Combining the mean value from Equation 3.3, the reference variance from Equation 3.5 and the evolution of the variance with the size and the reference variance from Equation 3.4, the evolution law of the cone of convergence, shown in Equation 3.2, is rewritten as shown in Equation 3.6

$$\ln y = \langle \ln \mu \rangle \pm \sqrt{\frac{V_{ref}}{V_s}}\sigma_{ref} \quad \Leftrightarrow \quad y = \mu \cdot \exp\left(\pm\sqrt{\frac{V_{ref}}{V_s}}\sigma_{ref}\right) \tag{3.6}$$

The Empirical Rule applies, which means that the number of standard deviations taken into account determines the amount of data which is fitted within the boundaries of the cone. One standard deviation is approximately 68% of the data, two standard deviations are around 95% and three standard deviations are approximately 99.7%. Since it is statistically possible to obtain outliers which could influence the

shape of the boundaries of the cone, we use twice the standard deviation in our fit.

$$y = \mu \cdot \exp\left(\pm 2\sqrt{\frac{V_{ref}}{V_s}}\sigma_{ref}\right) \tag{3.7}$$

In two dimensions, which is the case with the random packings, the volume is equal to the square of the length ($V_s = L_s^2$). And since the permeability and REV convergence is usually plotted with respect to the sample length, the evolution of the cone of the REV convergence is described as shown in Equation 3.8.

$$y = \mu \cdot \exp\left(\pm 2\frac{L_{ref}}{L_s}\sigma_{ref}\right) \tag{3.8}$$

Note that in three dimensions, which is usual when analysing real samples, the evolution of the cone is described as shown in Equation 3.9.

$$y = \mu \cdot \exp\left(\pm 2\left(\frac{L_{ref}}{L_s}\right)^{3/2}\sigma_{ref}\right) \tag{3.9}$$

Although we recommend that to take the homogenized values of the largest samples to describe the evolution law of the cone, we note that different sample sizes can be included as well, under the conditions that the samples are independent. The summation is then applied over different sample sizes (s) and observations within that sample size (n_j). This is rewritten so that the ratio of the size to the reference size is correlated to the observation.

$$\sigma_{ref}^2 \approx \frac{1}{n}\sum_{j=1}^{s}\frac{V_j}{V_{ref}}\sum_{i=1}^{n_j}\ln\left(\frac{x_i}{\langle x\rangle}\right)^2 = \frac{1}{n}\sum_{i=1}^{n}\frac{V_i}{V_{ref}}\ln\left(\frac{x_i}{\mu}\right)^2 \tag{3.10}$$

3.2.3. Fit of the determined evolution law

We calculate the variance and the mean value with the data points of the permeability and energy dissipation, and plot the evolution of the log-normal distributions, as described in Equation 3.8, in Figure 3.1. The boundaries of the distribution at two times the standard deviation are shown with a red line and the mean value with a red dashed line.

We observe that the mean value of the log-normal distribution aligns with the average mean value of the homogenized values. The boundaries of the log-normal distribution also align accurately with the boundaries of the cones of convergence. This confirms that fitting a log-normal distribution on the data points accurately describes the shape of the cone and can therefore be utilized to describe the convergence itself.

The fit of the convergence cones of the energy dissipation appears to exclude more outliers, compared to the cones of the permeability. Despite having similar proportions of data points fitting within the mathematical model with twice the standard deviation, the outliers of the convergence cone of the energy ratio are more visible as they appear near the start of the cone. We also observe that the cones of the energy show a steeper convergence, compared to the cones of permeability, from which we can conclude that the convergence of the energy ratio is slightly faster.

Although the general shape and evolution law of the cone of convergence is the same for each of the cones, we observe that the convergence depends on the porosity of the sample. Lower porosities present a wider base of the cone than higher porosities. For example, the width of the convergence cone of the energy ratio with a porosity of 53% is almost double the width of the cone with a porosity of 41%. The correlation between the reference variance and the porosity is shown in Figure 3.5.

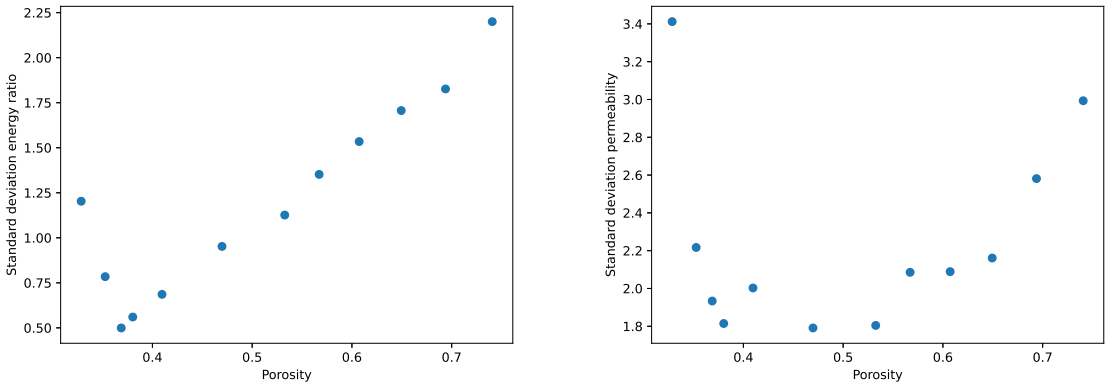

Figure 3.5: The evolution of the standard deviation compared to the porosities of the random packings. On the left the standard deviations of the energy ratio is shown, and the standard deviation of the permeability on the right.

The trend observed with the porosity confirms that the convergence for the permeability or energy dissipation ratio depends on the microstructural properties of the sample.

Since the evolution of the cone of convergence is accurately described by fitting a statistical model, in the form of a log-normal distribution, on the cones of convergence, we can utilize the properties of the statistical model and provide information about the error of the fit. On top of the number of data points taken into account and the decreasing variance, which provides information about the accuracy of the determined REV and homogenized property, the model also presents the error of the standard deviation (O'neill [32]), which on its turn is directly related to the width and convergence of the cone.

$$\frac{\epsilon}{\sigma} = \frac{1}{\sqrt{2N-2}} \tag{3.11}$$

The evolution of the accuracy is shown in Figure 3.6, which presents the reference standard deviation of the permeability for three different porosities and the number of models taken into account. The figure clearly shows the convergence towards a certain value and that the fluctuation around that value becomes smaller with the increase in the number of samples. Interestingly, we note from Equation 3.11 that the relative error does not depend on the actual size of standard deviation, but on the number of models taken into account. This means that the size of the sample is not influenced by the relative error and that the evolution law of the convergence, as described with the log-normal distribution, can be fitted with data from any sample size. The relative error also allows to calculate the number of models required to meet a predetermined accuracy.

3.3. Application to real microstructure

The previous section confirms the concept of the cone of convergence for the REV and shows that the generic evolution law of the convergence cone can be described by fitting the data points in a log-normal distribution. As the generic evolution law has been determined with idealized microstructures, we now verify if the evolution law also applies to real microstructures. Real microstructures contain natural heterogeneities which may affect the evolution of the cone of convergence. This section will analyse samples with increasing heterogeneity.

The process for reconstructing digital rocks follows the method proposed by [24]. 2D micro CT scans are segmented and translated into 3D computational models, where the rock and void space are distinguished. To minimize the computational expenses required for simulations, the Displaced Boundary method introduced by Lesueur, Rattez, and Colomés [23] is employed. This approach allows the pore-boundary interface to be conformed to a coarser background mesh, resulting in smaller mesh files.

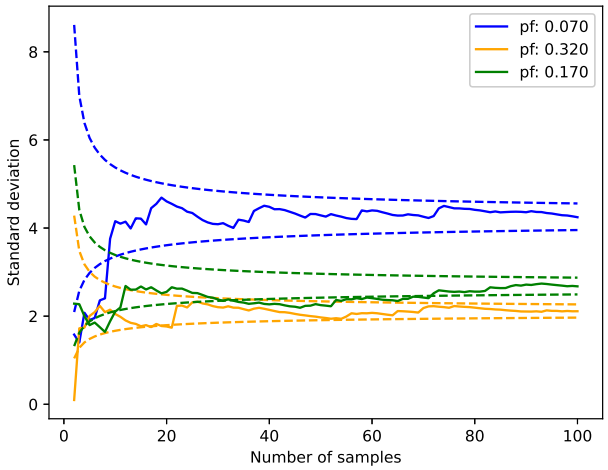

Figure 3.6: Three examples of the evolution of the reference standard deviation of the permeability with respect to the number of samples taken into account.

Whereas the random packings are virtually created and can therefore generate an unlimited amount of samples with the same characteristics, the CT-scanned microstructures provide limited data due to the maximum size of the sample and the scan resolution. To overcome this limitation in plotting the cone of convergence, the rock sample is split into multiple subsamples. To enforce that the subsamples still reflect the behaviour of the rock, the samples can-not be infinitely small. Therefore, each rock sample is cut into four equally sized parts in each direction, resulting in 64 subsamples. Bigger samples would result in a lower accuracy of the cone of convergence and smaller samples may not have reached the percolation threshold. The relative error of the base of the cone is 9%, which is calculated with Equation 3.11. The subsamples do not overlap to ensure that the post-processed permeability and energy dissipation are independent within each subsample.

The first rock sample in this study is the LV60A sand pack Pore-scale Imaging and Modelling [38], which is displayed in Figure 3.7a. While the sand pack is relatively homogeneous for a real rock sample, it still contains natural heterogeneities in the grain properties, such as grain roughness and non-sphericity. The sand pack has high permeability owing to the good connectivity of its voids, shown with a porosity of 38% and a characteristic length of 149 μm. These properties make it a good starting point for verifying the identified evolution law of the cone of convergence. The LV60A sand pack sample has a size of just over three mm and is scanned using a resolution of 10.008 μm, resulting in 300^3 voxels. The cones of convergence for both the permeability and energy dissipation of the sand pack are shown in Figure 3.7 b and c.

The results show that the determined evolution law of the cone fits the convergence of both the energy ratio and the permeability to a satisfying degree. The energy ratio cone is especially accurate near the bottom half and the permeability shows excellent representation overall. Again, the lack of population inside the cone can be explained by the lack of data points. The fit of the cone improves with larger samples, which can be explained by the decreased variance of the physical properties.

Compared to the random packings, we find that the general shape of the cone and the corresponding evolution law of the convergence cone is not affected by the grain heterogeneities. We do, however, observe a higher variance in both the energy dissipation and the permeability, compared to the random packings.

We utilize the evolution law of the cone of convergence to determine the permeability and the size of the REV and obtain values that align with those reported by Mostaghimi, Blunt, and Bijeljic [31]. The permeability is found to be 37 Darcy, which is around a five per cent margin of 39 Darcy noted by

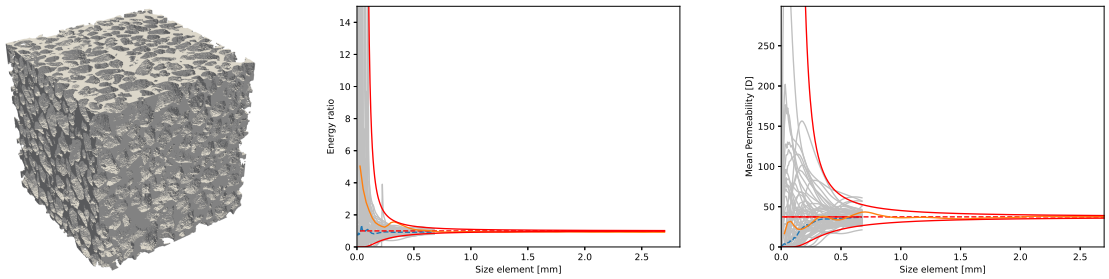

Figure 3.7: The results for the LV60A sandpack. On the left, the pore space of the sand pack is shown. The middle graph shows the convergence cone of the energy consistency. The right graph shows the convergence cone of the permeability of the rock sample. The grain lines in the graph show the variance of the property, the red lines show the cone of convergence and the blue line is a single tracing of the full sample.

Mostaghimi. Mostaghimi has shown that the REV is found at a length of 1.1 mm for the permeability, at which we measure an error of five per cent using the cone of convergence of the energy dissipation ratio.

The second sample in this study is the S1 sandstone Pore-scale Imaging and Modelling [39], shown in Figure 3.8a. Unlike sand packs, which consist of individual grains, sandstone is a type of rock with a cohesive structure in which the grains are cemented together by minerals. Sandstones tend to have lower permeability due to the lower connectivity of their voids and the more tortuous flow paths. As a result, the S1 Sandstone exhibits slightly more heterogeneous properties, shown with a porosity of 20% and a characteristic length of 311 μm, making it harder to find REV. The S1 sandstone is scanned with a resolution of 8.7 μm over a total length of just over 2.6 mm, resulting in 300^3 voxels. The cones of convergence for both the permeability and energy dissipation of the sandstone are shown in Figure 3.8 b and c.

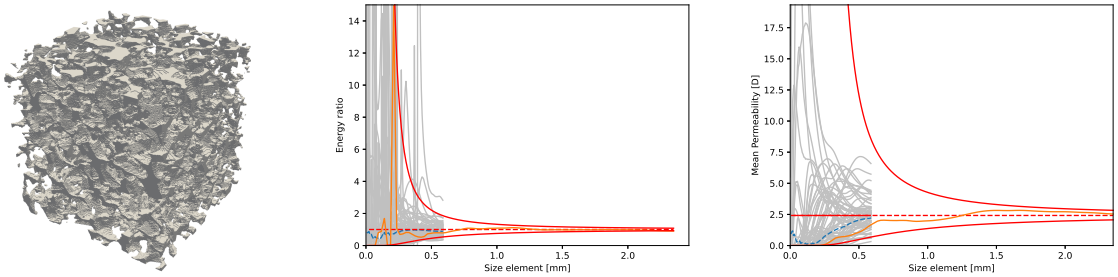

Figure 3.8: The results for the S1 sandstone. On the left, the pore space of the sandstone is shown. The middle graph shows the convergence cone of the energy consistency. The right graph shows the convergence cone of the permeability of the rock sample.

The results show that the lower connectivity of the voids does not influence the general shape of the cone of convergence. This means that the evolution of the cone can still be accurately described by the determined evolution law. The main difference we observe, compared to the sand pack and random packings, is the higher variance and corresponding slower convergence. The cone of the energy ratio is rather accurately described with the determined evolution law, as both the bottom and the top part are well populated. The permeability seems to obtain more values at the lower part, although the fit of the cone is still satisfying.

[31] has shown the REV to be around 1.3 mm in length size, yet there is still some evolution in the permeability. If we fit the evolution law of the cone of convergence, we find that at 1.3 millimeters, the error of the size of the permeability REV is around 11%.

The third sample in this study is the Ketton limestone Modelling [30], which is shown in Figure 3.9a.

Limestone is typically composed of calcium carbonate and is therefore often quite heterogeneous, with substantial variance in grain shapes and sizes and non-uniformly connected pore spaces. However, this particular limestone sample is relatively homogeneous and has reasonably well-connected voids, shown with a porosity of 13% and a characteristic length of 331 μm. The sample has a high-resolution CT scan image of three μm and with a total size of just over three mm, the digital reconstruction results in 1000^3 voxels. The cones of convergence for both the permeability and energy dissipation of the limestone are shown in Figure 3.9 b and c.

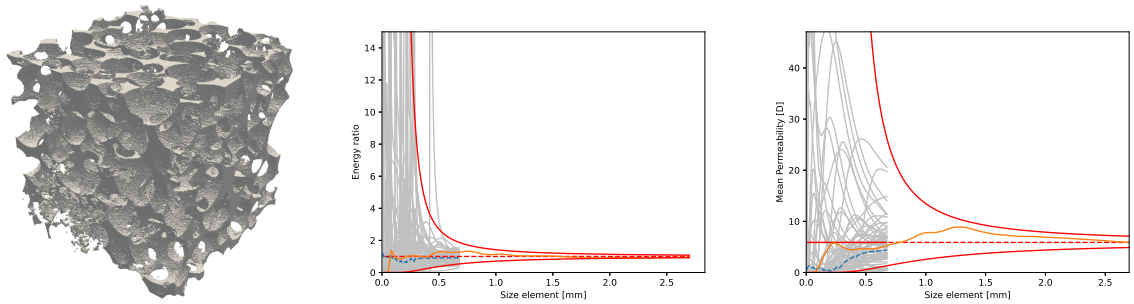

Figure 3.9: The results for the Ketton limestone. On the left, the pore space of the limestone is shown. The middle graph shows the convergence cone of the energy consistency. The right graph shows the convergence cone of the permeability of the rock sample.

The results of the Ketton simulation show many similarities to the results of the sandstone. The cone fits nearly perfectly on the convergence of the energy ratio and to satisfaction on the convergence of the permeability. The convergence of permeability is again mainly fitted using the lower part of the cone but shows a high variance in the beginning, which is included in the description of the cone.

If we aim for an error of ten per cent of the variance of the cone, we find that the Ketton limestone has a REV of around 1.2 mm. If a lower error of five per cent is considered, the REV would have a length of approximately 1.8 mm.

The final sample in this study is the C2 carbonate Pore-scale Imaging and Modelling [37], as shown in Figure 3.10a. This carbonate exhibits high heterogeneity in grain properties and low connectivity of voids, shown with a porosity of 14% and a characteristic length of 220 μm, resulting in low permeability overall. [31] showed that the REV size cannot be determined for permeability, even when the full sample is taken into account. However, by applying the principle of the cone of convergence, an estimation of the size of the REV is possible. The sample has an image resolution of 5.7 μm and a total size of just under 2.3 mm, which results in 400^3 voxels. The cones of convergence for the carbonate are presented in Figure 3.10 b and c.

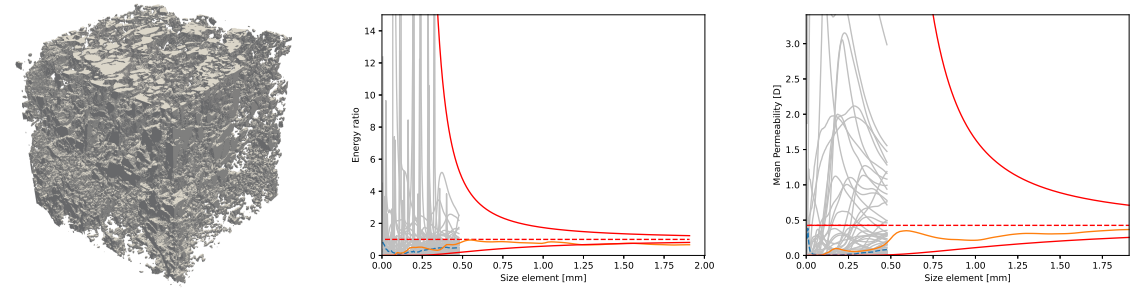

Figure 3.10: The results for the carbonate C2. On the left, the pore space of the carbonate is shown. The middle graph shows the convergence cone of the energy consistency. The right graph shows the convergence cone of the permeability of the rock sample.

The results show a very high variance compared to the other samples. Note that the percolation thresh-

old has not been fully reached yet within each subsample, and therefore the range of the homogenized properties is still high. The energy ratio still has a variance of over 18%.

Although the cone of convergence with the energy ratio is particularly well-fitted, we observe that the description of the convergence of the permeability is less accurate. Since the values of the permeability still range vary significantly within the maximum subsamples as the percolation threshold is not reached, the base of the cone is wide and may not accurately describe the convergence. We note that as the percolation threshold is reached with the other samples and the random packings, the convergence of the properties is quick and therefore easier to describe.

With the evolution law of the cone of convergence of the energy ratio, we predict that an error of ten per cent results in a REV size of 3.1 mm and an error of five per cent results in a REV with a length of 4.9 mm.

3.4. Requirements for the convergence cone

In the previous sections, we determined the generic evolution law of the cone of convergence with Random Packings and applied this law to real rock structures. We verified that the evolution law is still applicable, with natural heterogeneities included. As the cone of convergence allows to determine the REV and homogenized property without the need for large simulations, this chapter discusses the requirements of samples to fit an accurate cone and compares the application with traditional methods, computational and time-wise, to find REV.

3.4.1. Sample requirements

Section 3.2 presented that the accuracy of the fit is depended on the number of models taken into account. The variance of the distribution, which is directly related to the boundaries of the cone, and the mean value are estimated with the number of samples taken into account. We show that the error of the boundaries can be estimated with a relative error, which only depends on the number of samples. However, the absolute error depends also on the value of the variance.

This becomes clear in Section 3.3, especially with the C2 carbonate sample. The variance of the permeability is quite high and only 64 samples can be taken into account. This means that the fit of the cone became less accurate, compared to the random packings or other rock samples. In the other rock samples, the percolation threshold is reached, which decreases the range of the values significantly. This makes the absolute error of the fit lower and improves the fit of the cone of convergence.

For this reason, we advise fitting the cone of convergence with samples bigger than the percolation threshold, as these samples somewhat represent the overall behaviour of the flow within the full rock sample. Using a predetermined accuracy, it is possible to calculate the number of samples needed. When there is not enough data or amount of samples available, it is still possible to fit the cone of convergence and predict the size of the REV, albeit with lower accuracy.

When the data is limited, we also observe that the energy ratio index presents a more accurate fit of the cone of convergence. Not only is the converged value known to be unitary, but the cone itself is also better filled within the boundaries of the evolution law compared to the cone of REV convergence, which provides confirmation that the fit is correct. The fitted cone is then easily utilized to predict the size of the REV.

3.4.2. Computational requirements

To demonstrate the required computational resources to fit the cone of convergence, the LV60A sand pack is used as an example. The cone is fitted with a similar set-up as previously in Section 3.3, with the rock being divided into 64 subsamples. To get rid of the boundary effects, a slightly bigger subsample is taken for the simulation. The post-processing of the effective properties is done within a subsample, to get away from the boundary effects and to ensure we avoid overlap of the subsamples.

The computational requirements to plot the cone are compared to a traditional method of tracing the convergence of the REV, where the simulations are run on growing subsamples of the sand pack, up to the maximum size of 300^3 voxels. Both the simulation memory and time are traced throughout, which is shown in Figure 3.11.

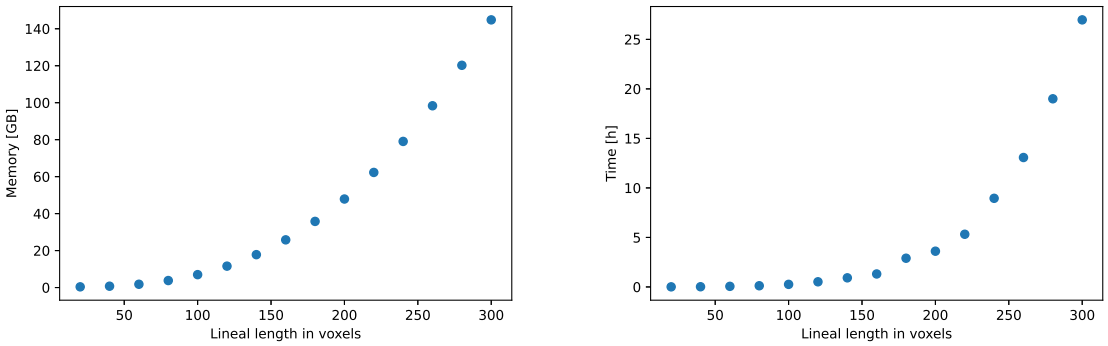

Figure 3.11: The two figures show the computational resources required to simulate Stokes flow in the LV60A sand pack for an increasing subsample. On the left, the trend between memory usage and the length of the sample is shown. On the right, the trend between simulation time and the length of the sample is displayed. The subsample size is shown in orange.

We observe that both the time and memory required for the simulation increase, following a higher-order power law. Whereas traditional methods require large simulations to verify whether the fluctuation of the property has damped out, the cone of convergence suffices simulations. The fourth, orange point on the graphs is equal to the size of the subsamples and it is clear that both the memory requirement and simulation time is significantly lower than the full sample.

Because the sample is split into subsamples, the simulation can be tweaked to the available resources. To put it into perspective, the full sample takes approximately 828 times longer than a single subsample and the memory requirement is reduced by a factor of 60. Running the simulations of all the subsamples at the same time would almost double the memory requirement, compared to simulating the full model, yet the process would run 828 times faster. Running all the simulations successive would, on top of the memory reduction of a factor of 60, still be four times faster. If we match the memory of the full sample, the subsamples can split into two batches and the simulation time would still be 100 times faster than the full model.

3.5. Conclusion

In conclusion, this paper has presented a study on finding the Representative Volume Element (REV) through the analysis of the convergence of both the permeability and the energy ratio index.

With Finite Element simulations of Stokes-flow through idealized microstructures, we present the convergence without the influences of heterogeneities. We show that the convergence follows a cone of convergence, with exponential growth and decay towards a converged value. The generic evolution law of the cone, therefore, be described by an exponential function, incorporating the mean value and variance of a log-normal distribution. We show that the proposed description of the cone accurately describes the boundaries of the cone and the converged value and can be used to determine the size of the REV. On top of that, the applied statistical log-normal distribution provides information about the error of the values, size of the REV and fit.

The evolution law of the convergence is applied to real rock samples, which include real heterogeneities. We validate that the same formulation can be used for the real samples, as the description matches the shape of the cone, despite the heterogeneities leading to a wider base of the cone. Moreover, we show that if the REV can-not be determined at the maximum size of the sample, a prediction for the

size of the REV and the associated physical properties can still be made by utilizing the evolution law of the cone of convergence.

Since the cone of convergence can be fitted with both idealized microstructures and real rock samples, we show that it is possible to speed up the process of finding the REV. With a large number of small simulations, dependent on a predetermined accuracy and the percolation threshold, it is possible to adjust the process to the computational resources required and available. The traditional large simulations required to find REV, which costs the most computational resources and time, are not necessary anymore.

4

Conclusion and recommendations

4.1. Conclusion for the homogenization without the influence of the boundary conditions

The first part of this thesis has studied the process of upscaling physical properties, specifically the permeability, from a rock microstructure to a homogenized parameter for the macroscale. This is a process based on the postulation of the Hill-Mandel principle of energy consistency throughout the transition of scales. Traditional homogenization methods apply specific boundary conditions to enforce energy consistency. Yet, it has been found that boundary conditions influence the property of the rock sample. Although, applied homogenization within a subsample, away from the boundary layer, will provide the effective property. With the latter in mind, this study has focused on finding the natural energy consistency in the intrinsic subsample.

With the results of Stokes-flow simulations through idealized microstructures of random packings, the energy ratio index from micro- to macro-scale is analysed. With a convergence towards a stable value of one, it is determined that the energy consistency can be found at the size of the Representative Elementary Volume (REV). Therefore, the homogenization still complies with the Hill-Mandel principle and the effective property of the rock can be upscaled from the microstructure to the macro-structure in a valid matter, without the influence of the boundary condition. The results of the idealized microstructure are extended to real rock microstructures, to validate whether the results are still valid with natural heterogeneities included. It is shown that the energy consistency is still found at REV, although with a slower convergence. From this, it is concluded that it is possible to apply homogenization by tracing the convergence of the energy ratio, without enforcing the energy consistency with boundary conditions. On top of that, the unitary value for the energy ratio index provides for an accurate indicator of whether REV has been found.

It is shown that without the REV the energy consistency cannot be established and hence it is not always possible to apply valid homogenization. Carbonates, for example, tend to be quite heterogeneous, which makes it challenging to find the REV and establish energy consistency throughout the transition of scales.

4.2. Recommendations for the homogenization without the influence of the boundary conditions

To ensure the wider applicability of this research, we recommend extending the analysis to different physical properties. For example, if energy consistency can be demonstrated within a subsample considering different physical phenomena, such as mechanics or electrics, it can be concluded that the effective properties of a rock sample can be determined for a broad field of interest.

To use the suggested method of homogenization, it is now required to determine the size of the boundary layer for each sample. Future research could characterize the size of the boundary layer with the

morphological properties of the microstructure. For example, when the random packings are assessed, it is shown that the size of the boundary layer does depend on the porosity of the rock structure. If a generic relation between the size and the morphological properties can be determined, the boundary layer does not need to be determined for each sample. The types of boundary conditions can be taken into account as well.

Another topic of interest for future work is to study the difference between the convergence of the REV for energy consistency and the REV for permeability. It is shown and confirmed by the second part of this thesis, that the REV for the permeability is a larger volume than for the energy consistency, although with a small difference.

4.3. Conclusion for the evolution law of the convergence for REV

The second part of this thesis studied the process of finding the REV. Finding the REV is a crucial aspect of homogenization and upscaling, as it behaves as a representative medium. Yet, the determination of the size of the REV is a challenging exercise, which traditionally includes many and large simulations to trace the convergence towards a certain parameter and takes up a large number of computational resources and time. As is shown in numerical statistical studies and the previous part of the research, the convergence towards the REV and physical parameters follows the shape of a cone. This part of the thesis aimed to find the generic evolution law of the convergence for the REV and utilize it to predict the size of the REV and the homogenized property.

To find the generic evolution law, the cones of convergence for the REV for both the energy ratio index and the permeability are presented for idealized microstructures. After analysing the shape of the convergence, it was shown that the generic evolution law of the convergence is described with the log-normal distribution for each sample size. The evolution of the REV convergence is described with the evolution of the variance, which can be described with a reference value, using the law of large numbers. The determined law is applied to the presented convergence of the permeability and energy ratio index for the random packings and is found to be an excellent fit, as the boundaries and the mean values described with the mathematical formulation align with the cone. This enables the determination of the size of the REV and the effective property with a number of simulations depending on a predetermined accuracy, without the need for large simulations.

This study is extended to real rock microstructures to verify whether the determined generic evolution law is applicable when natural heterogeneities are included. It is shown that the evolution law still predicts the convergence of the real microstructures. The increasing heterogeneity of the samples leads to a higher variation of the physical property, which is shown to be accurately captured with the log-normal distribution. Even when the size of the REV is not reached within the full size of the sample, a prediction of the size and physical properties can be made, utilizing the evolution law of the cone of convergence.

It is shown that the cone of convergence is more accurately described when the percolation threshold is reached within a subsample. This also influences the accuracy of the determined evolution law of the convergence cone, as the variation of the physical quantities is large. As a result, the percolation threshold provides the minimum size of the subsamples which should be taken into account and the number of samples influence the accuracy of the fit.

Lastly, it is shown that the computational time and resources follow a higher-order power law, with respect to the size of the sample. By running a number of simulations of smaller volumes, this power law will reduce to a linear function. The splitting of the sample into subsamples also unlocks the possibility to work with high-resolution samples, which were previously too computationally demanding for simulations.

4.4. Recommendations for the evolution law of the convergence for REV

The evolution law is currently determined for an intrinsic, average property in the form of permeability for the rock sample. Before using it for different physical quantities, it would be useful to validate the method for those quantities, such as the stiffness, strength or conductivity.

Another interesting topic would be to study the size of the samples which is needed to set up the cone of convergence in more detail. The conclusions of the research recommend using samples which include the percolation threshold of the rock sample and taking as many samples as possible to fit the cone of convergence as well as possible. More insight into the samples might lead to a better recommendation for the size of the samples needed to find the REV.

The cone of convergence is fitted with just two parameters, namely the variance and the mean value of the log-normal distribution. It is already shown in previous research that the variation of the convergence is an indicator of the heterogeneity of a rock sample (Rahman et al. [41]). If the variation and mean value can be described with the morphological parameters of a microstructure, the size of the REV and the homogenized property becomes superfluous, as these can be predicted with the determined evolution law of the convergence.

Overall, this thesis presents both a new method to apply valid homogenization and a new method to determine the size of the REV and the homogenized physical property. These methods combined present a new method to apply fast and valid homogenization, without influences of the boundaries and the need for large simulations.

References

[1] Douglas G Altman and J Martin Bland. “Standard deviations and standard errors”. In: *BMJ* 331.7521 (Oct. 2005), p. 903. DOI: 10.1136/bmj.331.7521.903.

[2] Heiko Andrae et al. “Digital rock physics benchmarks—part II: Computing effective properties”. In: *Computers and Geosciences* 50 (Jan. 2013), pp. 33–43. DOI: 10.1016/j.cageo.2012.09.008.

[3] J.-L. Auriault. “Heterogeneous periodic and random media. Are the equivalent macroscopic descriptions similar?” In: *International Journal of Engineering Science* 49.8 (Aug. 2011), pp. 806–808. DOI: 10.1016/j.ijengsci.2011.01.005.

[4] Branko Bijeljic et al. “Predictions of non-Fickian solute transport in different classes of porous media using direct simulation on pore-scale images”. In: *Physical Review E* 87.1 (Jan. 2013), p. 013011. DOI: 10.1103/physreve.87.013011.

[5] Oistein Boe. “Analysis of an upscaling method based on conservation of dissipation”. In: *Transport in Porous Media* 17.1 (1994), pp. 77–86. DOI: 10.1007/bf00624051.

[6] Antonio Cancelliere et al. “The permeability of a random medium: Comparison of simulation with theory”. In: *Physics of Fluids A: Fluid Dynamics* 2.12 (Dec. 1990), pp. 2085–2088. DOI: 10.1063/1.857793.

[7] Philip Crosbie Carman. “Fluid flow through granular beds”. In: *Trans. Inst. Chem. Eng.* 15 (1937), pp. 150–166.

[8] Melissa R. Cox and Muniram Budhu. “A practical approach to grain shape quantification”. In: *Engineering Geology* 96.1-2 (Jan. 2008), pp. 1–16. DOI: 10.1016/j.enggeo.2007.05.005.

[9] P. K. Weyl D. C. Beard. “Influence of Texture on Porosity and Permeability of Unconsolidated Sand”. In: *AAPG Bulletin* 57 (1973). DOI: 10.1306/819a4272-16c5-11d7-8645000102c1865d.

[10] X Du and M Ostoja-Starzewski. “On the size of representative volume element for Darcy law in random media”. In: *Proceedings of the Royal Society A: Mathematical, Physical and Engineering Sciences* 462.2074 (Apr. 2006), pp. 2949–2963. DOI: 10.1098/rspa.2006.1704.

[11] Alex A. Elvin. “Number of grains required to homogenize elastic properties of polycrystalline ice”. In: *Mechanics of Materials* 22.1 (Jan. 1996), pp. 51–64. DOI: 10.1016/0167-6636(95)00024-0.

[12] Kirill M. Gerke, Marina V. Karsanina, and Regina Katsman. “Calculation of tensorial flow properties on pore level: Exploring the influence of boundary conditions on the permeability of three-dimensional stochastic reconstructions”. In: *Physical Review E* 100.5 (Nov. 2019), p. 053312. DOI: 10.1103/physreve.100.053312.

[13] Christophe Geuzaine and Jean-François Remacle. “Gmsh: A 3-D finite element mesh generator with built-in pre- and post-processing facilities”. In: *International Journal for Numerical Methods in Engineering* 79.11 (May 2009), pp. 1309–1331. DOI: 10.1002/nme.2579.

[14] Christophe Geuzaine and Jean-François Remacle. “Gmsh: A three-dimensional finite element mesh generator with built-in pre-and post-processing facilities”. In: 79 (Nov. 2008).

[15] I.M. Gitman, H. Askes, and L.J. Sluys. “Representative volume: Existence and size determination”. In: *Engineering Fracture Mechanics* 74.16 (2007), pp. 2518–2534. ISSN: 0013-7944. DOI: https://doi.org/10.1016/j.engfracmech.2006.12.021. URL: https://www.sciencedirect.com/science/article/pii/S0013794406004772.

[16] S Graham and N Yang. “Representative volumes of materials based on microstructural statistics”. In: *Scripta Materialia* 48.3 (Feb. 2003), pp. 269–274. DOI: 10.1016/s1359-6462(02)00362-7.

[17] Quentin Grimal et al. “A determination of the minimum sizes of representative volume elements for the prediction of cortical bone elastic properties”. In: *Biomechanics and Modeling in Mechanobiology* 10.6 (Jan. 2011), pp. 925–937. DOI: 10.1007/s10237-010-0284-9.

[18] Romain Guibert et al. “A Comparison of Various Methods for the Numerical Evaluation of Porous Media Permeability Tensors from Pore-Scale Geometry”. In: *Mathematical Geosciences* 48.3 (Mar. 2015), pp. 329–347. DOI: 10.1007/s11004-015-9587-9.

[19] R. Hill. “Elastic properties of reinforced solids: Some theoretical principles”. In: *Journal of the Mechanics and Physics of Solids* 11.5 (Sept. 1963), pp. 357–372. DOI: 10.1016/0022-5096(63)90036-x.

[20] T. Kanit et al. “Determination of the size of the representative volume element for random composites: statistical and numerical approach”. In: *International Journal of Solids and Structures* 40.13-14 (June 2003), pp. 3647–3679. DOI: 10.1016/s0020-7683(03)00143-4.

[21] Josef Kozeny. “Uber kapillare leitung der wasser in boden”. In: *Royal Academy of Science, Vienna, Proc. Class I* 136 (1927), pp. 271–306.

[22] Thomas E. Lacy, David L. McDowell, and Ramesh Talreja. “Gradient concepts for evolution of damage”. In: *Mechanics of Materials* 31.12 (Dec. 1999), pp. 831–860. DOI: 10.1016/s0167-6636(99)00029-0.

[23] Martin Lesueur, Hadrien Rattez, and Oriol Colomés. “MicroCT scans permeability computation with an unfitted boundary method to improve coarsening accuracy”. In: *Computers and Geosciences* 166 (Sept. 2022), p. 105118. DOI: 10.1016/j.cageo.2022.105118.

[24] Martin Lesueur et al. “Modelling fluid-microstructure interaction on elasto-visco-plastic digital rocks”. In: *Geomechanics for Energy and the Environment* 12 (Dec. 2017), pp. 1–13. DOI: 10.1016/j.gete.2017.08.001.

[25] Cheng Liu. “On the minimum size of representative volume element: An experimental investigation”. In: *Experimental Mechanics* 45.3 (June 2005), pp. 238–243. DOI: 10.1007/bf02427947.

[26] Dariusz Łydżba and Adrian Różański. “Microstructure measures and the minimum size of a representative volume element: 2D numerical study”. In: *Acta Geophysica* 62.5 (June 2014), pp. 1060–1086. DOI: 10.2478/s11600-014-0226-5.

[27] J. Mandel. “Plasticité classique et viscoplasticité: course held at the department of mechanics of solids”. In: *courses and lectures - International Centre for Mechanical Sciences Springer-Verlag;New York, NY: 1972.* (1972).

[28] Ester Marafini et al. “Suitability of 2D modelling to evaluate flow properties in 3D porous media”. In: *Transport in Porous Media* 134.2 (July 2020), pp. 315–329. DOI: 10.1007/s11242-020-01447-4.

[29] S.M. Mirkhalaf, F.M. Andrade Pires, and Ricardo Simoes. “Determination of the size of the Representative Volume Element (RVE) for the simulation of heterogeneous polymers at finite strains”. In: *Finite Elements in Analysis and Design* 119 (Oct. 2016), pp. 30–44. DOI: 10.1016/j.finel.2016.05.004.

[30] Imperial College Consortium On Pore-Scale Modelling. “Ketton Limestone”. In: (). URL: https://imperialcollegelondon.app.box.com/v/iccpsim-ketton2015.

[31] Peyman Mostaghimi, Martin J. Blunt, and Branko Bijeljic. “Computations of Absolute Permeability on Micro-CT Images”. In: *Mathematical Geosciences* 45.1 (Dec. 2012), pp. 103–125. DOI: 10.1007/s11004-012-9431-4.

[32] B O’neill. “Some Useful Moment Results in Sampling Problems”. In: *The American Statistician* 68.4 (Oct. 2, 2014), pp. 282–296. DOI: 10.1080/00031305.2014.966589.

[33] Catherine Teresa Paéz-García, Francisco J. Valdés-Parada, and Didier Lasseux. “Macroscopic momentum and mechanical energy equations for incompressible single-phase flow in porous media”. In: *Physical Review E* 95.2 (Feb. 2017), p. 023101. DOI: 10.1103/physreve.95.023101.

[34] C. Pelissou et al. “Determination of the size of the representative volume element for random quasi-brittle composites”. In: *International Journal of Solids and Structures* 46.14-15 (July 2009), pp. 2842–2855. DOI: 10.1016/j.ijsolstr.2009.03.015.

[35] Cody J. Permann et al. “MOOSE: Enabling massively parallel multiphysics simulation”. In: *SoftwareX* 11 (2020), p. 100430. ISSN: 2352-7110. DOI: https://doi.org/10.1016/j.softx.2020.100430. URL: http://www.sciencedirect.com/science/article/pii/S2352711019302973.

[36] John W. Peterson, Alexander D. Lindsay, and Fande Kong. “Overview of the incompressible Navier–Stokes simulation capabilities in the MOOSE framework”. In: *Advances in Engineering Software* 119 (May 2018), pp. 68–92. DOI: 10.1016/j.advengsoft.2018.02.004.

[37] Imperial College Consortium on Pore-scale Imaging and Modelling. “C2 carbonate”. In: (Oct. 2014). DOI: 10.6084/m9.figshare.1189258.v1. URL: https://figshare.com/articles/dataset/C2_carbonate/1189258.

[38] Imperial College Consortium on Pore-scale Imaging and Modelling. “LV60A sandpack”. In: (Oct. 2014). DOI: 10.6084/m9.figshare.1153795.v2. URL: https://figshare.com/articles/dataset/LV60A_sandpack/1153795.

[39] Imperial College Consortium on Pore-scale Imaging and Modelling. “S1 sandstone”. In: (Oct. 2014). DOI: 10.6084/m9.figshare.1189274.v1. URL: https://figshare.com/articles/dataset/S1_sandstone/1189274.

[40] A. Pouya and O. Fouche. “Permeability of 3D discontinuity networks: New tensors from boundary-conditioned homogenisation”. In: *Advances in Water Resources* 32.3 (Mar. 2009), pp. 303–314. DOI: 10.1016/j.advwatres.2008.08.004.

[41] Taufiq Rahman et al. “Representative Elementary Volume of Rock Using X-Ray Microcomputed Tomography: A New Statistical Approach”. In: *Geofluids* 2020 (Sept. 2020), pp. 1–13. DOI: 10.1155/2020/8866486.

[42] Z.-Y. Ren and Q.-S. Zheng. “Effects of grain sizes, shapes, and distribution on minimum sizes of representative volume elements of cubic polycrystals”. In: *Mechanics of Materials* 36.12 (Dec. 2004), pp. 1217–1229. DOI: 10.1016/j.mechmat.2003.11.002.

[43] Ph. Renard and G. de Marsily. “Calculating equivalent permeability: a review”. In: *Advances in Water Resources* 20.5-6 (Oct. 1997), pp. 253–278. DOI: 10.1016/s0309-1708(96)00050-4.

[44] Paul K. Romano et al. “OpenMC: A state-of-the-art Monte Carlo code for research and development”. In: *Annals of Nuclear Energy* 82 (Aug. 2015), pp. 90–97. DOI: 10.1016/j.anucene.2014.07.048.

[45] S.K. Sebsadji and K. Chouicha. “Determining periodic representative volumes of concrete mixtures based on the fractal analysis”. In: *International Journal of Solids and Structures* 49.21 (Oct. 2012), pp. 2941–2950. DOI: 10.1016/j.ijsolstr.2012.05.017.

[46] Zhaohui Shan and Arun M Gokhale. “Representative volume element for non-uniform microstructure”. In: *Computational Materials Science* 24.3 (June 2002), pp. 361–379. DOI: 10.1016/s0927-0256(01)00257-9.

[47] Jianwei Shi et al. “On the Influence of Boundary Conditions when Determining Transport Coefficients from Finite Samples of Porous Media: Assessment for Tomographic Images of Real Materials”. In: *Transport in Porous Media* 132.3 (Mar. 2020), pp. 561–590. DOI: 10.1007/s11242-020-01404-1.

[48] Jean-François Thovert and Valeri V. Mourzenko. “On the influence of boundary conditions when determining transport coefficients from digital images of heterogeneous media.” In: *Advances in Water Resources* 141 (July 2020), p. 103612. DOI: 10.1016/j.advwatres.2020.103612.

[49] E. V. Torskaya et al. “Mechanical and tribological properties of nanostructured coatings based on multicomponent oxides”. In: *Journal of Friction and Wear* 34.2 (Mar. 2013), pp. 99–106. DOI: 10.3103/s1068366613020141.

[50] Stephen Whitaker. “Flow in porous media I: A theoretical derivation of Darcy’s law”. In: *Transport in Porous Media* 1.1 (1986), pp. 3–25. DOI: 10.1007/bf01036523.

[51] T.R. Zakirov and M.G. Khramchenkov. “Study of the pore space heterogeneity effect on the absolute permeability tensors calculated under different boundary conditions and driving forces using a “Computational Rock Physics” technology”. In: *Journal of Petroleum Science and Engineering* 216 (Sept. 2022), p. 110750. DOI: 10.1016/j.petrol.2022.110750.

[52] Tao Zhu et al. “A Study of the Time Constant in Unsteady Porous Media Flow Using Direct Numerical Simulation”. In: *Transport in Porous Media* 104.1 (May 2014), pp. 161–179. DOI: 10.1007/s11242-014-0326-3.

[53] S. Zwarts and M. Lesueur. “Homogenization method based on energy conservation and independent of boundary conditions”. In: (2023).

A

Stokes-flow model set-up

In this appendix, details for the model set-up created in the research for conducting Stokes-flow calculations are provided.

A.1. Microstructures

For the idealized microstructures random packings containing perfectly round spheres of the same diameter are created with the OpenMC Monte Carlo code (Romano et al. [44]). Using spheres ensures that the grains are perfectly round and the microstructure does not contain grain heterogeneities. The porosity of the microstructure is controlled by the packing fraction, which determines the number of spheres inside the predetermined volume. To save memory, a two-dimensional cross-section is taken of the random packing as the representation of the microstructure. This is done by cutting the resulting disk of the two-dimensional representation out of the square volume. As shown in Figure A.1, this results in the void space on which a flow can be imposed.

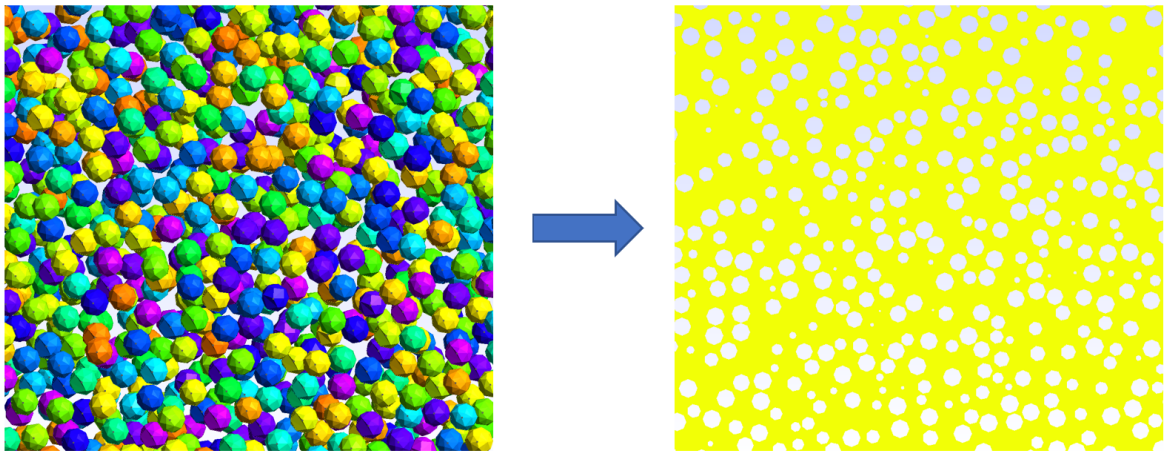

Figure A.1: Visualisation of the transition of a three-dimensional random packing, a volume filled with spheres, to a two-dimensional representation of the void space.

The process for the real rock microstructures follows the traditional steps of Digital Rock Physics. The three-dimensional computational model of a rock sample is created with a series of images obtained with CT scanning. These images are then processed to filter and segment the images into the void space and the solid matrix material of the rock. Once the segmentation is complete, the images are reconstructed together to create a three-dimensional model of the rock sample. Once the three-dimensional model is created, the void space can be meshed to run finite element simulations of Stokes-flow. This process of reconstruction is visualised in Figure A.2.

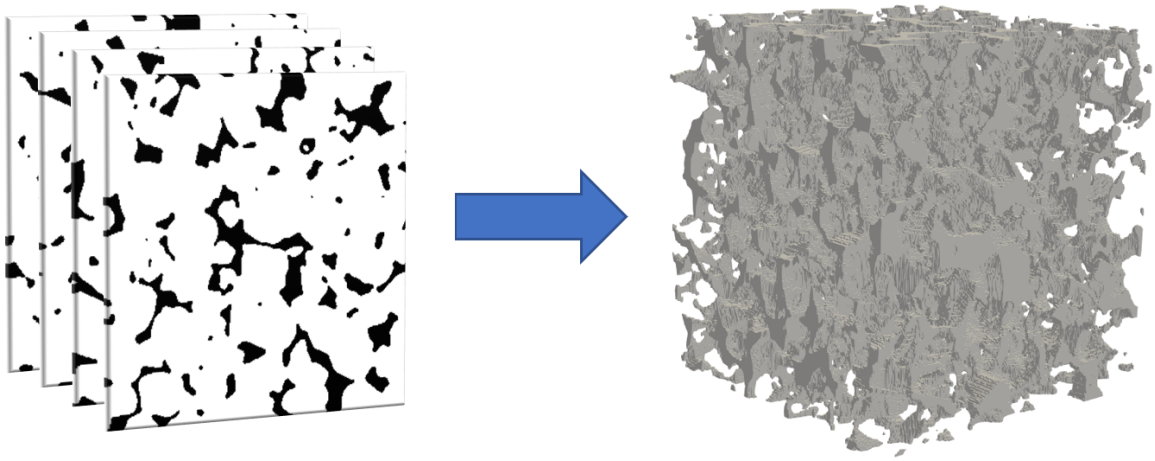

Figure A.2: Visualisation of the reconstruction of micro CT images to a computational microstructure.

A.2. Mesh

To numerically simulate fluid flow through random packings using the Finite Element Method, the void space is discretized into a mesh grid of smaller elements, specifically triangular first-order elements.

A.2.1. Meshing random packings

GMSH (Geuzaine and Remacle [14]) is used to create the mesh for the random packings, which generates a mesh grid with the mesh size as input.

During the mesh convergence study with a homogeneous mesh grid, it was observed that the size of the mesh files increases significantly with higher packing fractions. When the random packing is made with a high packing fraction, the domain contains more disks. The boundary of the disks is circular, which is difficult to represent with triangular elements and therefore requires a smaller element size, which results in a larger mesh file. For example, the mesh file with packing fractions over 52% exceeds 10 GB. Running simulations on these large mesh files is challenging, as they require a significant amount of computational resources and time. To reduce the mesh-file size, a study of different mesh grids is performed.

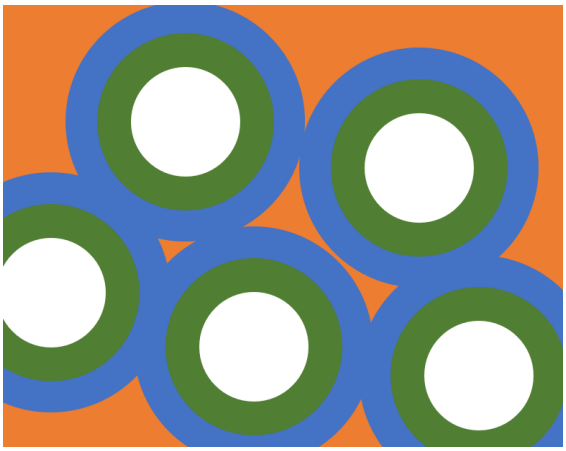

Figure A.3: Representation of the different mesh fields and mesh structure for GMSH. The green region is the field of the boundary of the circle, the blue region is the transition field and the orange region is the void field.

Since the representation of the disks is the most critical factor affecting the mesh size, mesh refinement around the boundary of the disks is examined using three different mesh fields: the boundary of the circle, the transition field, and the void field, as shown visually in Figure A.3.

The field of the boundary of the circles contains smaller mesh elements to accurately describe the circular shape of the grains. The mesh in the void space contains bigger elements since it is assumed that the size of the element in the void space does not influence the result of the mesh convergence as much. As the difference between the two different mesh fields can become large, a transition field is applied to match the two different element sizes together. The proportion of each field is depended on input parameters, defining how many columns of mesh element are fitted within each field. An example of how this is implemented is shown in the Python code snippet below and in Figure A.4.

The Python code for setting up the different fields in the mesh configuration for GMSH

```
"""
Setting up the different fields for the mesh configuration.
x is the maximum mesh resolution of the void field
y is the number of elements which represent the size of the transition field
"""

gmsh.model.mesh.field.add("Distance", 1)
gmsh.model.mesh.field.setNumbers(1, "CurvesList", [seq[1] for seq in grains])

gmsh.model.mesh.field.add("Threshold", 2)
gmsh.model.mesh.field.setNumber(2, "InField", 1)
gmsh.model.mesh.field.setNumber(2, "SizeMin", resolution)
gmsh.model.mesh.field.setNumber(2, "SizeMax", resolution*x)
gmsh.model.mesh.field.setNumber(2, "DistMin", 0)
gmsh.model.mesh.field.setNumber(2, "DistMax", resolution*y)

gmsh.model.mesh.field.add("Min", 3)
gmsh.model.mesh.field.setNumbers(3, "FieldsList", [2])
gmsh.model.mesh.field.setAsBackgroundMesh(3)
```

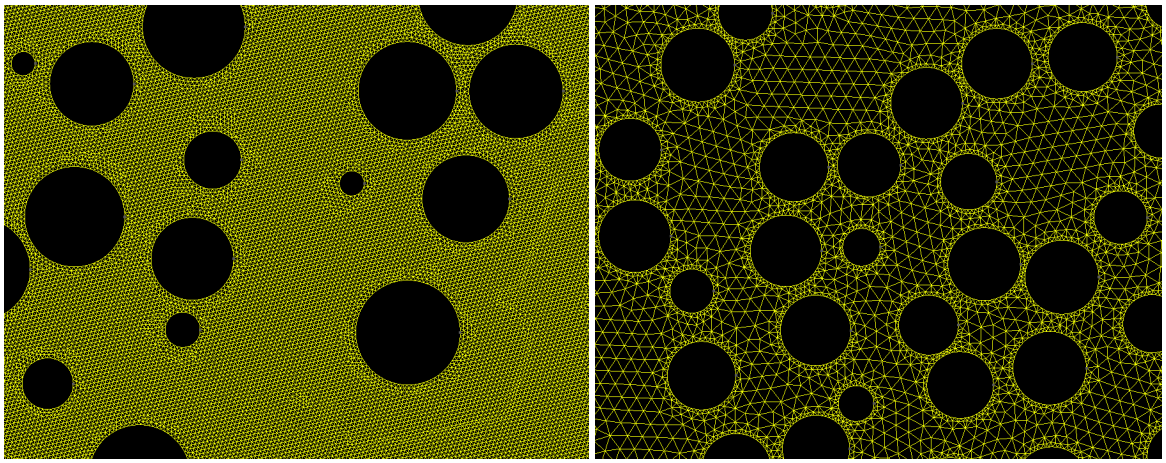

Figure A.4: Visualisation from the meshes, with the uniform mesh grid on the left and the heterogeneous mesh on the right. Both the grids are from the same packing fraction of 27% and use the same mesh element size near the boundary of the circle.

The performance of the different mesh fields was evaluated by comparing the number of mesh elements needed for mesh convergence with the number of elements in a uniform grid with a homogeneous mesh element size. The comparison is shown in Figure A.5, where a boundary field with a width of three mesh elements and a void field with mesh elements five times larger than the boundary field is used.

The results show that the initial convergence towards mesh convergence is steeper with the different mesh fields. This is especially noticeable with the higher packing fractions, which include more circles in the mesh configuration. However, it is also observed that the mesh convergence has a trend towards the same number of elements. Therefore the actual difference in file size between the two methods

when mesh convergence is reached is neglectable. For the sake of the stability of the simulations, only homogeneous meshes are applied in the mesh configuration.

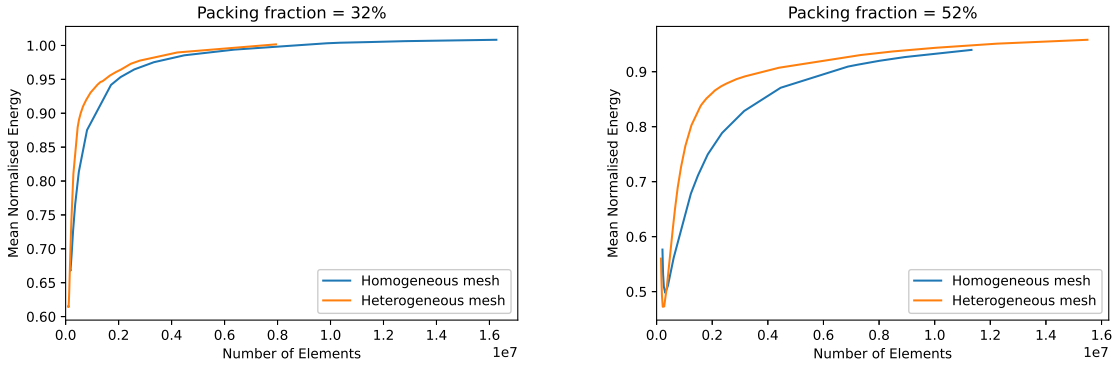

Figure A.5: The comparison between the different mesh structures, with the blue line representing the mesh convergence with a homogeneous mesh size and the orange line representing the mesh convergence with the different mesh fields included. On the left, the mesh convergence for a lower packing fraction of 32% is shown, on the right the mesh convergence with a higher packing fraction of 52% is presented.

A.2.2. Meshing real microstructures

The real microstructures are meshed with the displaced boundary method, as described in Lesueur, Rattez, and Colomés [23]. The meshes for real microstructures can become large, as some microstructures require a highly refined mesh. The displaced boundary method obtains a definition of the pore-grain interface as precise as traditional methods but with coarser meshes. In summary, the method uses the input of the geometry of the microstructure, to redistribute the nodes of the mesh grid to the boundary of the geometry and therefore uses fewer elements to accurately describe the complicated pore-boundary interface.

A.3. Stokes-flow module

To find the permeability and energy dissipation of the fluid, Stokes-flow is simulated on the microstructures. Stokes flow is a simplification of the Navier-Stokes equations, which are equations describing the momentum balance and the conservation of mass. By assuming a lack of body forces and an incompressible fluid, the differential equations are as follows:

$$\mu \nabla^2 u - \nabla p = 0 \tag{A.1}$$

$$\nabla \cdot u = 0 \tag{A.2}$$

To impose the flow in the microstructure, the pressure on opposites sides is defined, with values of zero and one, as shown in Figure A.6. This means we have a constant pressure gradient over the sample. The top and bottom boundaries have a predetermined boundary of zero velocity in both directions with no-slip conditions, or only zero velocity in the vertical direction with slip conditions. The boundaries of the grains have no-slip conditions, implemented by a value of zero velocity in both vertical and horizontal directions. Both the fluid density (ρ) and the dynamic viscosity (μ) are set to one.

The numerical part and mathematics of the implementation of Stokes-flow in MOOSE are explained in [35] and Peterson, Lindsay, and Kong [36]. In summary, one of the main sources of instability in Finite Element simulations of Stokes flow is the so-called pressure-velocity coupling instability. MOOSE uses a stabilized version of the Petrov-Galarkin Finite Element Method, which adds a stabilization term to the weak formulation of the flow equations to ensure the stability of the solution of the flow through the microstructure. An example of how the result looks is presented in Figure A.7.

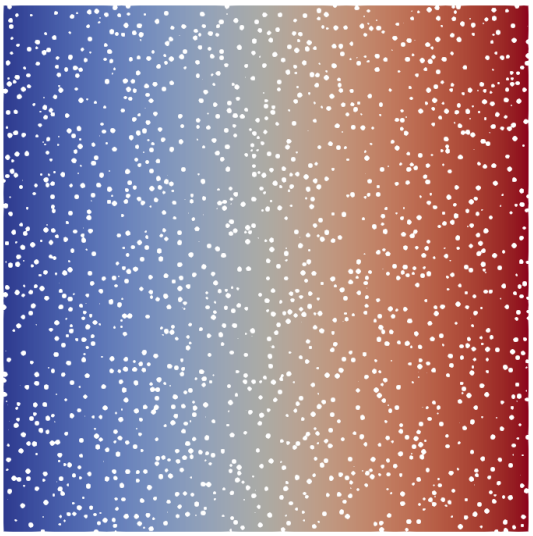

Figure A.6: The pressure graphically shown on the microstructure. The blue colour on the left is equal to a pressure of zero and the red colour on the right represents a pressure of one.

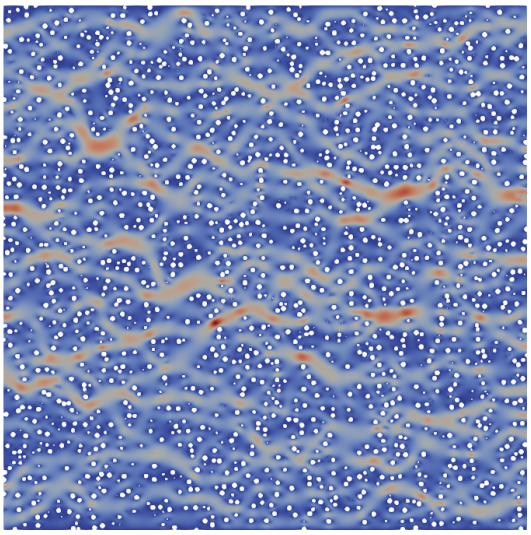

Figure A.7: The result of Stokes-flow inside a microstructure. The example shown is a random packing with a packing fraction of 27%.